For 2nd Symposium on Accelerator Dosimetry
and Experience, Stanford, Ca., November 5-7, 1969

UCRL-19391
Preprint

c. 2

RECEIVED
LAWRENCE
RADIATION LABORATORY
JAN 22 1970
LIBRARY AND
DOCUMENTS SECTION

STOPPING POWER, RANGE, AND TERMINAL IONIZATION OF ANY NUCLEUS WITH 0.01 TO 500 MeV/amu IN ANY NONGASEOUS MATERIAL, INCLUDING NUCLEAR EFFECTS

Roger Wallace, Gerald M. Litton, and Palmer G. Steward

November 1969

AEC Contract No. W-7405-eng-48

TWO-WEEK LOAN COPY

This is a Library Circulating Copy which may be borrowed for two weeks. For a personal retention copy, call Tech. Info. Division, Ext. 5545

UCRL-19391 Cy. 2

LAWRENCE RADIATION LABORATORY
UNIVERSITY of CALIFORNIA BERKELEY

DISCLAIMER

This document was prepared as an account of work sponsored by the United States Government. While this document is believed to contain correct information, neither the United States Government nor any agency thereof, nor the Regents of the University of California, nor any of their employees, makes any warranty, express or implied, or assumes any legal responsibility for the accuracy, completeness, or usefulness of any information, apparatus, product, or process disclosed, or represents that its use would not infringe privately owned rights. Reference herein to any specific commercial product, process, or service by its trade name, trademark, manufacturer, or otherwise, does not necessarily constitute or imply its endorsement, recommendation, or favoring by the United States Government or any agency thereof, or the Regents of the University of California. The views and opinions of authors expressed herein do not necessarily state or reflect those of the United States Government or any agency thereof or the Regents of the University of California.

STOPPING POWER, RANGE, AND TERMINAL IONIZATION OF ANY NUCLEUS WITH 0.01 TO 500 MeV/amu IN ANY NONGASEOUS MATERIAL, INCLUDING NUCLEAR EFFECTS

Roger Wallace, Gerald M. Litton, and Palmer G. Steward

University of California
Lawrence Radiation Laboratory
Berkeley, California

April 29, 1969

SUMMARY

Several methods are combined to provide the range, stopping power and Bragg peak data for any heavy ion with energy lying between 0.01 and 500 MeV per amu when incident on any nongaseous stopping medium. A Fortran IV program providing both numerical data and machine plots is available, so that any new particle or new stopping medium whether an element or a compound can be quickly evaluated in detail.

For ions at low energy with $Z \leq 10$, the program uses experimental data. For ions with $Z \geq 10$, the nuclear and electronic stopping-power theory developed by Lindhard et al. is adjusted to fission-product range data at low energy; for intermediate energies, charge-state data developed from experimental Ar range-energy data in Al is extended to other ions and stopping media. Bethe's theory is used for all ions at high energy. Bloch's theory is discussed, although it is not used in the method.

The particle ranges calculated by the method are pathlength ranges and do not include the effects of multiple scattering.

Using the calculated range energy and energy loss data, a method is described to calculate Bragg curves, flux curves, and energy spectra. Energy loss from electronic and nuclear elastic collisions, nuclear attenuation, small-angle multiple scattering, straggling initial energy, and angular spreads of the beam are all taken into consideration. Contributions from secondary particles have been estimated.

It is found that for a given range in a particular target, the peak-to-plateau dose ratio goes through a maximum as the atomic number of incident ions increases. Similarly, the Bragg peak full width at half-maximum goes through a minimum. In addition for a given range, the average energy per atomic mass unit at the Bragg peak is nearly independent of the bombarding ion, and also of the target material.

Calculated results agree well with experimental data for those cases in which secondary-particle production is of minor importance. Even when secondaries are a large contributing factor, the method yields valuable information regarding the variation in energy deposition by the primary particles. The results are found to be quite sensitive to the degree of angular and energy spread of the initial beam.

STOPPING POWER, RANGE, AND TERMINAL IONIZATION OF ANY NUCLEUS WITH 0.01 TO 500 MeV/amu IN ANY NONGASEOUS MATERIAL, INCLUDING NUCLEAR EFFECTS

Roger Wallace, Gerald M. Litton, and Palmer G. Steward

University of California
Lawrence Radiation Laboratory
Berkeley, California

Part I. Stopping Power and Range

1. Introduction

The purpose of the research reported in Part I is to provide estimates of the stopping power and ranges of all charged particles from hydrogen through uranium to any specific energy up to four to five hundred MeV/amu.

Throughout this paper we refer to MeV/amu, represented by the symbol ε, as a unit of specific energy. It is a unit intermediate between velocity and energy. The relationship to velocity is given by:

$$\varepsilon = 931\left[(1-\beta^2)^{-1/2}-1\right], \text{ or}$$

$$\beta = \frac{\frac{\varepsilon}{931}\left(\frac{\varepsilon}{931}+2\right)^{1/2}}{\frac{\varepsilon}{931}+1} ;$$

and the relationship to energy is given by:

$$\varepsilon = \frac{E}{A_1} .$$

The slowing-down mechanism of a charged particle in matter is similar throughout any plane of constant velocity in (V, Z_1, Z_2) space. Since ε is a function of velocity only, the same statement can be made regarding any plane of constant specific energy in (ε, Z_1, Z_2) space. This statement cannot be made for a plane of constant energy in (E, Z_1, Z_2) space. In this paper, we use specific energy as the independent variable rather than velocity or energy. Thus we use a unit which is a natural variable of the stopping-power process in the

same sense that velocity is, while at the same time we have a simple relationship between this unit and a common unit of energy.

We find it convenient in this report to discuss information in terms of (ε, Z_1, Z_2) space. For instance in Fig. 1 the slabs covering the bottom and part of the back of the box represent the volume of this space for which present accelerators can provide heavy particles. Alpha particles, as indicated in the figure, can be accelerated by the 184-Inch Synchrocyclotron to 230 MeV/amu. Protons, represented by the bottom slab, although only shown up to 500 MeV, can be accelerated far above 500 MeV. The computational method incorporated into our computer programs can supply stopping power and range data for Z_1 and Z_2 greater than 92 and for ε up to 1200 MeV/amu. In this paper, however, the boundaries of the space we consider are given by: $0.01 \leq \varepsilon \leq 500$, $1 \leq Z_1 \leq 92$, $1 \leq Z_2 \leq 92$. The slab along the back of the box describes the capabilities of the Hilac at Berkeley, which can give ions with $Z_1 \lesssim 20$ a specific energy of up to 10.4 MeV/amu.

Using this (ε, Z_1, Z_2) space as a device for restating the purpose of this research, we may say that it is our aim in this report, to provide a computational method for filling the box in Fig. 1 with range and stopping-power data. The range we calculate is the total path-length mean range and does not take into consideration the shortening of the projected range due to coulomb multiple scattering.

Relative dose, particle energy spectrum, LET spectrum and beam width all are calculated as a function of depth by means of introducing the effects of straggling, removal of particles due to nuclear collisions, and multiple coulomb scattering, thus the characteristics of the Bragg peak are determined.

The approximate limits of the only useful experimental stopping-power or range data available are illustrated in Fig. 1. The three slabs of (ε, Z_1, Z_2) space in which experimental stopping power has been accumulated by means of presently accelerated particles are shown. The two lines on the back of the box in Fig. 1 represent experimental fission product range values in aluminum and uranium respectively. Since the experimental data from these small regions must be extrapolated throughout the entire volume of the box, it is clear that the first guideline must be to include enough physical theory in order to make this extrapolation effective. The theory that we normalize to the experimental data is general enough to allow extrapolation to remote regions of (ε, Z_1, Z_2) space.

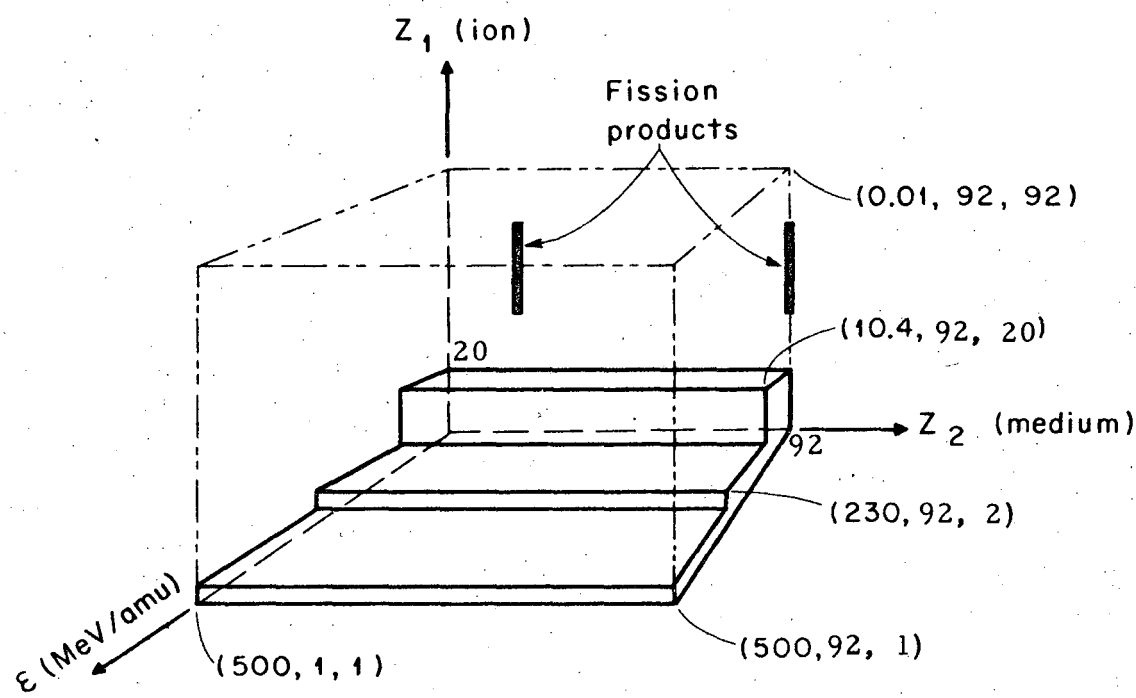

Fig. 1. A geometric view of that part of (ε, Z_1, Z_2) space for which $0.01 \leq \varepsilon \leq 500$, $1 \leq Z_1 \leq 92$, and $1 \leq Z_2 \leq 92$. The regions of this subspace for which experimental stopping power is available are indicated by the slabs covering the bottom and part of the back of the box (accelerated particle data) and the two lines on the back of the box (fission product range data).

2. Theory

The interactions of energetic heavy charged particles with matter has been of great interest for over half a century. Bohr developed the semi-classical stopping-power theory using impact parameters in 1913.[1,2] Bethe published his purely quantum mechanical theory in 1930.[3,4]

Each of those theories is valid in only part of the (ε, Z_1, Z_2) space. Bohr's theory is valid only when the following inequalities are satisfied.[5]

$$Z_2 \ll 137\beta, \tag{1}$$

$$(Z_2^2 r Z_1)^{1/3} \ll 137\beta, \tag{2}$$

$$\frac{\hbar}{mV} \ll \text{screening distance of scattering atom, and} \tag{3}$$

$$r Z_1 \gg 137\beta, \tag{4}$$

The screening distance of an atom is the distance from its nucleus to the radius where the screening by its electron cloud has reduced the effective nuclear charge to 1/e of its true value.

The expression 137β is the ion velocity in units of the Bohr orbital K shell velocity of the hydrogen atom. When discussing the interactions of charged particles with matter, this is a very convenient unit of velocity. Since the K shell electron velocity of the one-electron atom is proportional to the charge of the nucleus, inequality (1) can be restated: "In order for Bohr's theory to be valid, the velocity of the ion must be greater than the K shell electron velocity of the stopping medium." Similarly, inequality (4) limits the ion velocity to less than its own K shell electron velocity. Therefore Bohr's theory is limited to that region of (ε, Z_1, Z_2) space where the ion carries along with it its own electron cloud. This limits the usefulness of Bohr's theory to the few cases for which adequate charge-state data is available.

Bethe's theory is limited by the less restrictive of

$$r Z_1 \ll Z_2 \tag{5}$$

or

$$r Z_1 \ll 137\beta \tag{6}$$

Thus, since the K shell velocity of the ion is approximately $\beta = Z_1/137$ the use of Bethe's theory is essentially restricted to the region of (ε, Z_1, Z_2) space where the ion is completely ionized; although for very low energy when $r \sim 0$ the theory is again valid.

The Block[6] theory is restricted by

$$(Z_2 r Z_1)^{1/2} \ll 137\beta \tag{7}$$

in addition to inequality (1).

Bloch's theory provides a bridge between Bethe's and Bohr's theories in the sense that Bloch's theory agrees with Bohr's theory in the limit of inequality (4) and with Bethe's theory in the limit of inequality (6).

The usefulness of any of these theories is limited for $137\beta \leq Z_1$ because for these low velocities the ion carries along its own electron cloud. Lindhard, et al.[7,8] have recently developed the only generally useful theory valid at low ion velocities. Lindhard has made use of the Thomas-Fermi description of the electron clouds of the ion and stopping atom to give a formula for the stopping power due not only to excitation and ionization of the stopping atoms, but also to the elastic coulomb collisions of ion and nucleus of the stopping atom. The volume of (ε, Z_1, Z_2) space for which this theory is valid is given by

$$Z_1 \text{ and } Z_2 \gg 1 \text{ and} \tag{8}$$

$$Z_1^{1/3} \geq 137\beta. \tag{9}$$

In Fig. 2 we illustrate the volume of (ε, Z_1, Z_2) space in which each of the above four theories is valid. The boundaries separating each of the regions are somewhat arbitrarily placed. Lindhard's theory is valid over a plane across most of the back of the box. (It is actually a slab of thickness given by $0.01 \lesssim \varepsilon \lesssim 0.5$ MeV/amu). Bethe's theory with shell corrections is valid throughout perhaps a third of the box. It is valid over essentially all of the box for which r is unity. There is a small region in which Bloch's or Bohr's theory is valid and Bethe's theory is not valid. However, in this region r is less than one and uncertain. Thus the advantage of Bloch's or Bohr's theory over Bethe's in any region of the box is questionable. It is clear, at any rate, that over a large portion of the box there is no valid theory and no experimental data (see Fig. 1).

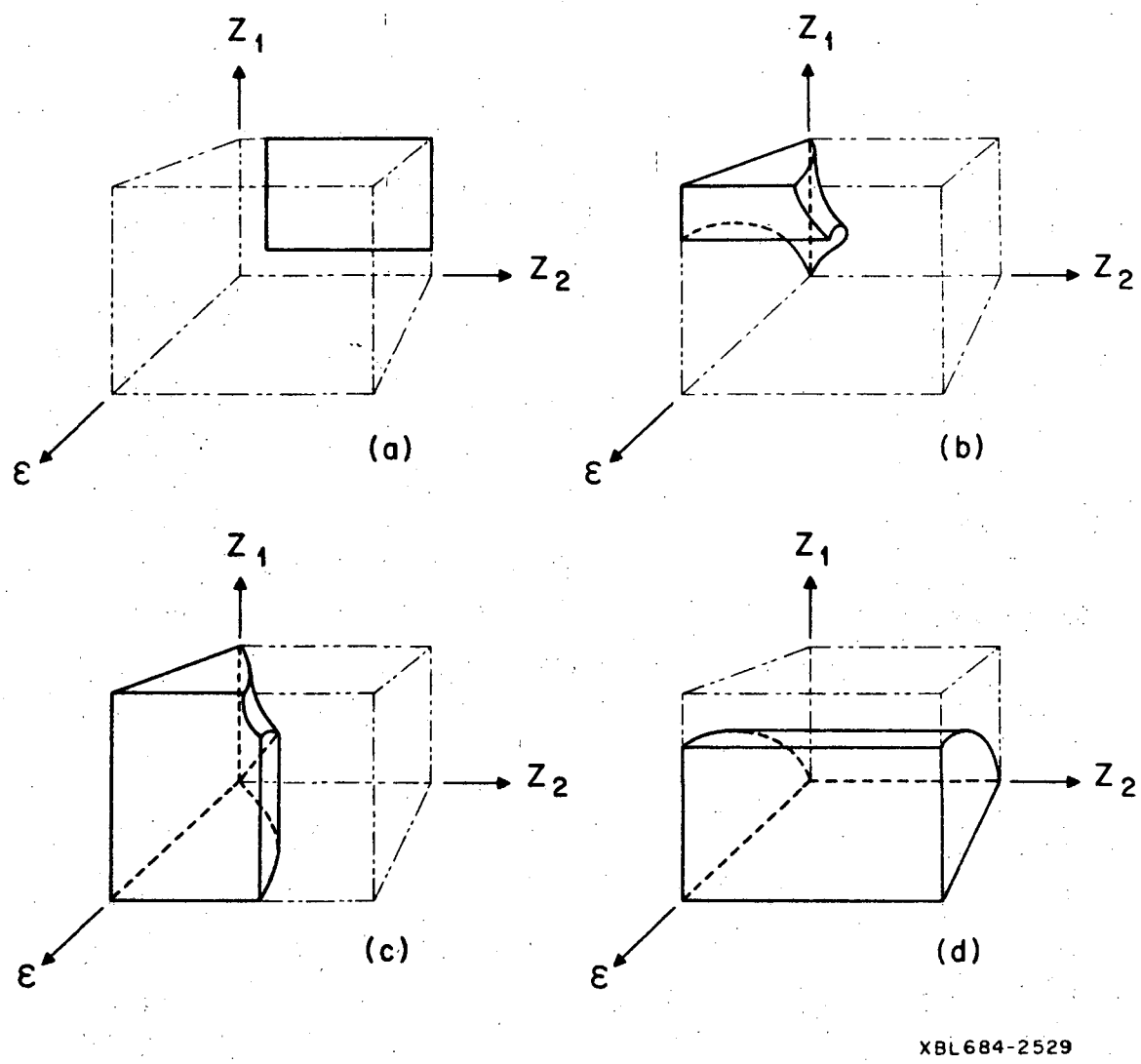

Fig. 2. In these four views of (ε, Z_1, Z_2) space we depict the regions of validity of four different theories. The theories are: (a) Lindhard et al.[8] ; (b) Bohr[1,2] ; (c) Bloch[6] ; and (d) Bethe[3,4].

4. These Calculations

The unique aspect of the research reported here is that nowhere else has stopping power and range been generated for such a large continuous volume of (ε, Z_1, Z_2) space where active charge exchange between ion and stopping medium occur. We have generated stopping power and ranges for all ions from hydrogen through uranium in any nongaseous stopping medium over the velocity interval from 0.01 to 500 MeV/amu continuously. Over this velocity interval the charge on the ion varies from less than 10% to 100% of its nuclear charge. The dE/dR maximum is contained in this interval for all ions. The generation of accurate stopping power for the very heavy ions in the region of dE/dR maximum is at this time a difficult undertaking. The technique developed here is a first order attempt to supply this data.

There have been several efforts to produce stopping power tables for use by researchers, but these tables usually do not give values which are valid for that difficult and large region of (ε, Z_1, Z_2) space in which active charge exchange occurs. (See ref. (13)).

In developing our method for generating stopping power, it is convenient for us to divide (ε, Z_1, Z_2) space into four regions. We develop for each region its own technique and strive for continuity in stopping power at the boundaries. The first boundary is the plane $Z_1 = 10$. For $Z_1 \leq 10$ experimental data are generally available where active charge exchange occurs. It is important to utilize these data, because it is not possible to treat this region well theoretically. Experimental data for $Z_1 > 10$ is very incomplete.

We subdivide the region defined by $Z_1 \leq 10$ into two subregions. For $\varepsilon < 10$ MeV/amu and $Z_1 \leq 10$ we make maximum use of experimental data from the Hilac and similar accelerators. We devise a technique in this subregion for generating stopping power which is not theoretically rigorous, but which does accurately duplicate available experimental data. Experimental data compiled by Northcliffe[10] is heavily relied upon in this region. For $\varepsilon \geq 10$ MeV/amu and $Z_1 \geq 10$, the ion is completely stripped of electrons and the application of Bethe's theory is straightforward. A polynomial fit to Bethe's theory developed by Barkas and Berger[9] is used.

We subdivide the region defined by $Z_1 > 10$ into four subregions. In the low-specific-energy region defined by $137\,\beta \leq Z_1^{1/3}$, we generate stopping power using Lindhard's[7,8] theories which are very slightly modified to conform to experimental fission product range data obtained from Hyde[11] and Aras.[12] Into the narrow medium-low-specific-energy

region defined by $Z_1^{1/3} < 137\beta \leq 9$ we merely extend the data generated in the adjacent regions by means of a polynomial function. In the medium-high-specific-energy region defined by $9 < 137\beta \leq 3Z_1$ we develop a technique for estimating the charge state of the heavy ions as a function of velocity, $r(\beta)$. We then obtain the stopping power using this charge state with Bethe's theory. In the high-specific-energy region, defined by $137\beta > 3Z_1$, the ion is again completely stripped of its electrons and Bethe's theory is used.

5. Results

The computer program described by Steward[13] has generated a sampling of ranges and stopping powers, some of which are displayed in this section. The ions chosen are hydrogen, helium^4, carbon^{12}, neon^{20}, argon^{40}, krypton^{84}, xenon^{131}, and radon^{222}. Data are presented for each of these ions incident upon water and uranium.

In Figs. 3 and 4 stopping power is plotted as a function of specific energy. The increasing contributions of the nuclear coulomb stopping-power term as Z_1 increases and ε decreases causes the slope of the curves to decrease under these conditions. According to Lindhard et al.[8] the assumption that the nuclear and electronic stopping powers are separable may lead to a systematic overestimation of the stopping power in this low-specific-energy region. The smoothed experimental stopping power which we try to duplicate with our method for $Z_1 \leq 10$ does not usually show a decreasing slope for decreasing velocity because the scatter of the experimental points is usually too great to permit the resolution of such fine detail. Thus the decreasing slope for decreasing velocity may be overestimated for Ar ions and underestimated for Ne ions, leading to a discontinuity in the systematic change of behavior across the $Z_1 = 10$ boundary.

In Figs. 5 and 6 the stopping power is plotted as a function of ion residual pathlength range. Points of constant specific energy are indicated by symbols at 0.01, 0.1, and 1.0 MeV/amu and by curves at 5, 10, 50, 100, 200, 300, and 500 MeV/amu. From Fig. 5, for instance, we see that a 5 MeV/amu ^{20}Ne in water has a LET of 7500 MeV/(g/cm^2) and a range of 100 microns. The discontinuity in behavior across the $Z_1 = 10$ boundary discussed above is apparent here also.

The H-He, C-Ne, and Xe-Rn crossovers of Fig. 5 are not as bizarre as they probably appear, because velocity and not residual range is the natural variable of stopping power. The reasons for these crossovers, which are possibly artifacts of the calculational technique, are discussed by Steward.[13]

In Figs. 7 and 8 the velocity is plotted as a function of residual range. The discontinuity in the systematic change of behavior across the $Z_1 = 10$ boundary, as discussed above, is apparent in these curves below 0.1 MeV/amu.

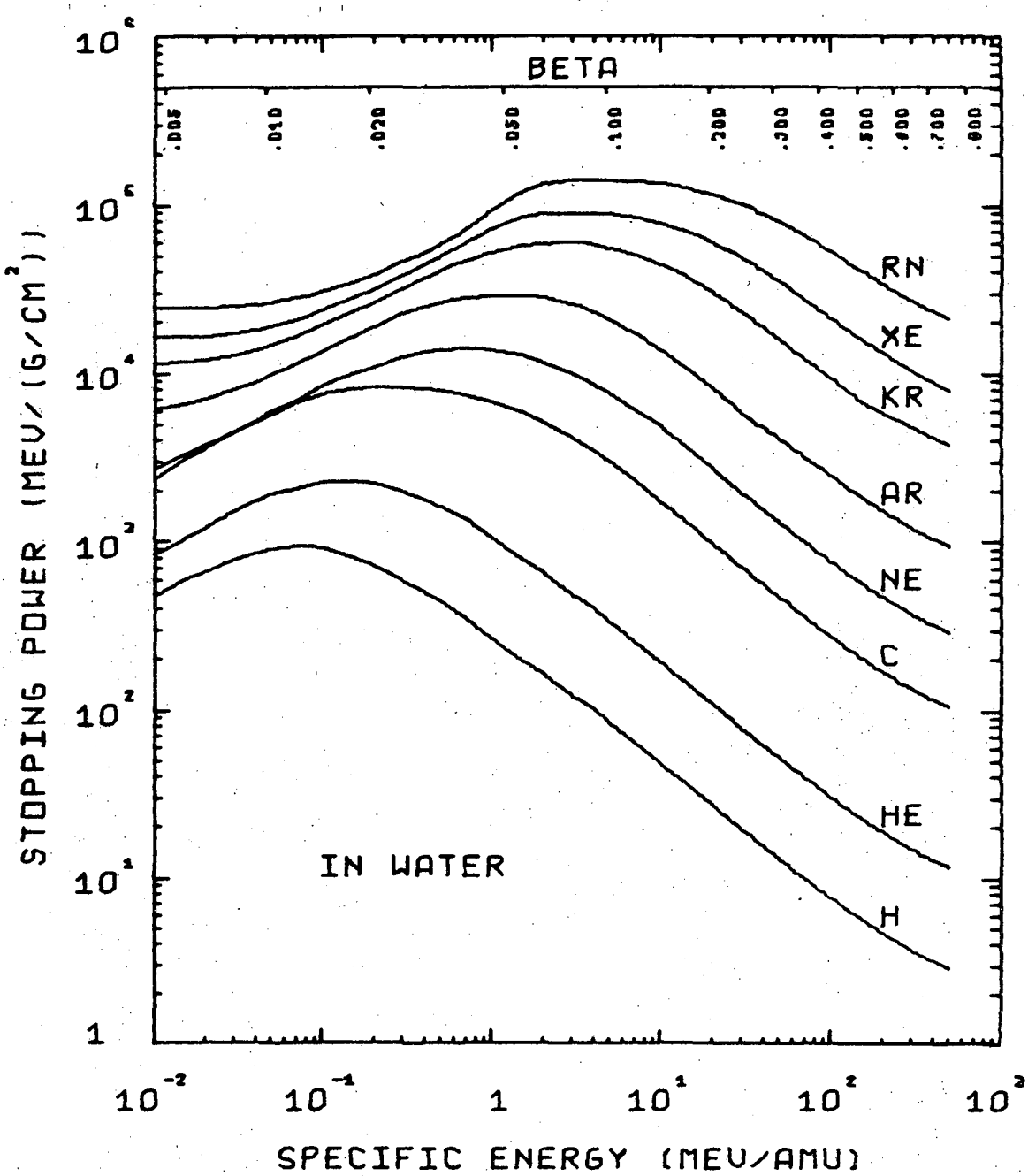

XBL 685-840

Fig. 3. Stopping-power curves as a function of specific energy for various ions in water as calculated by the computer program. At the top of the figure, values of $\beta = V/c$ are displayed. The Ne and C curves touch at about 0.04 MeV/amu due to an inaccuracy in the program which is apparent from Table VIC and D. Our method overestimates the experimental stopping power for carbon ions in hydrogen at 0.04 MeV/amu by 14% and underestimates it for Ne ions by 6%.

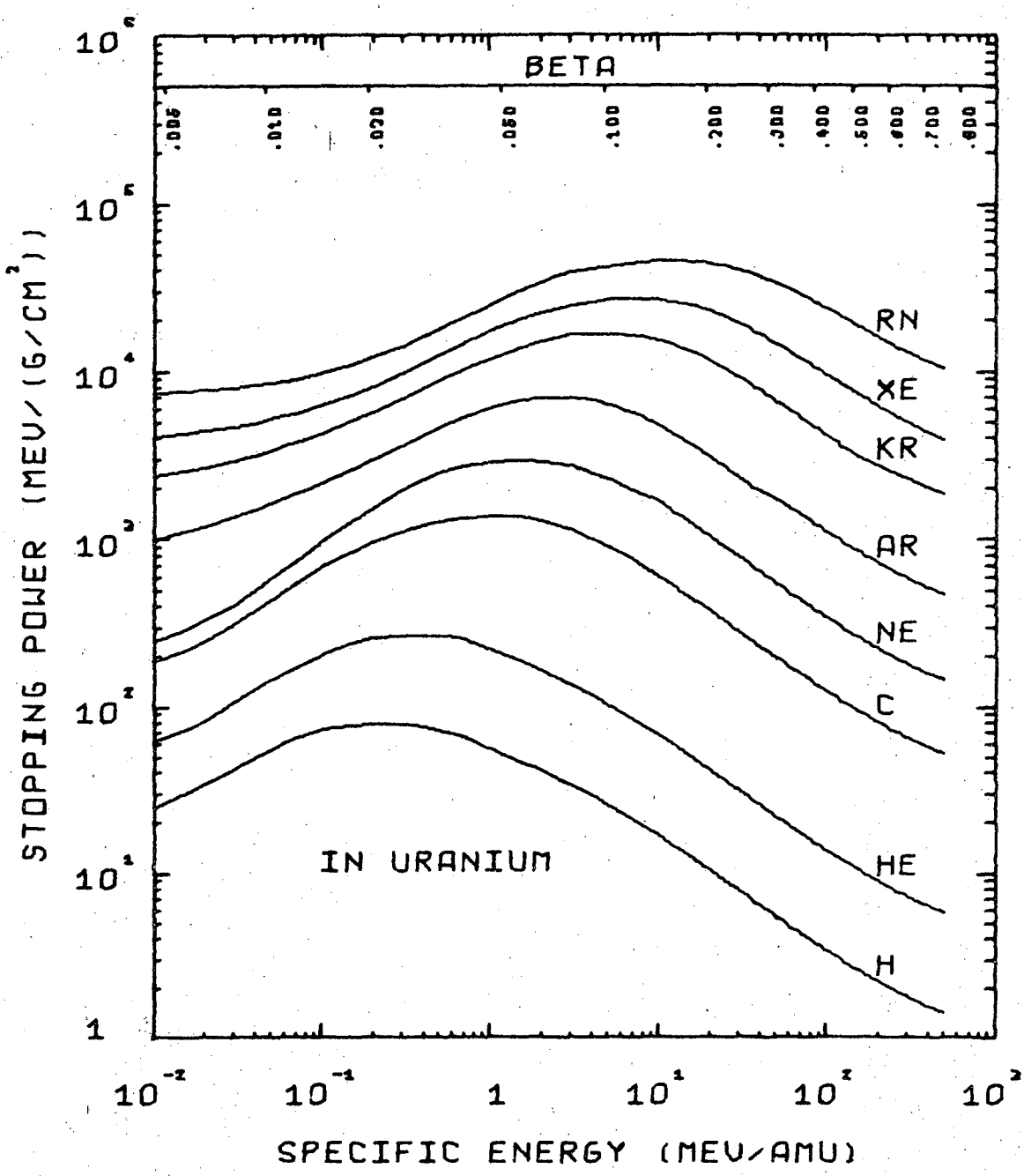

XBL 685-845

Fig. 4. Stopping-power curves as a function of specific energy for various ions in uranium as calculated by the computer program. At the top of the figure, values of $\beta = V/c$ are displayed.

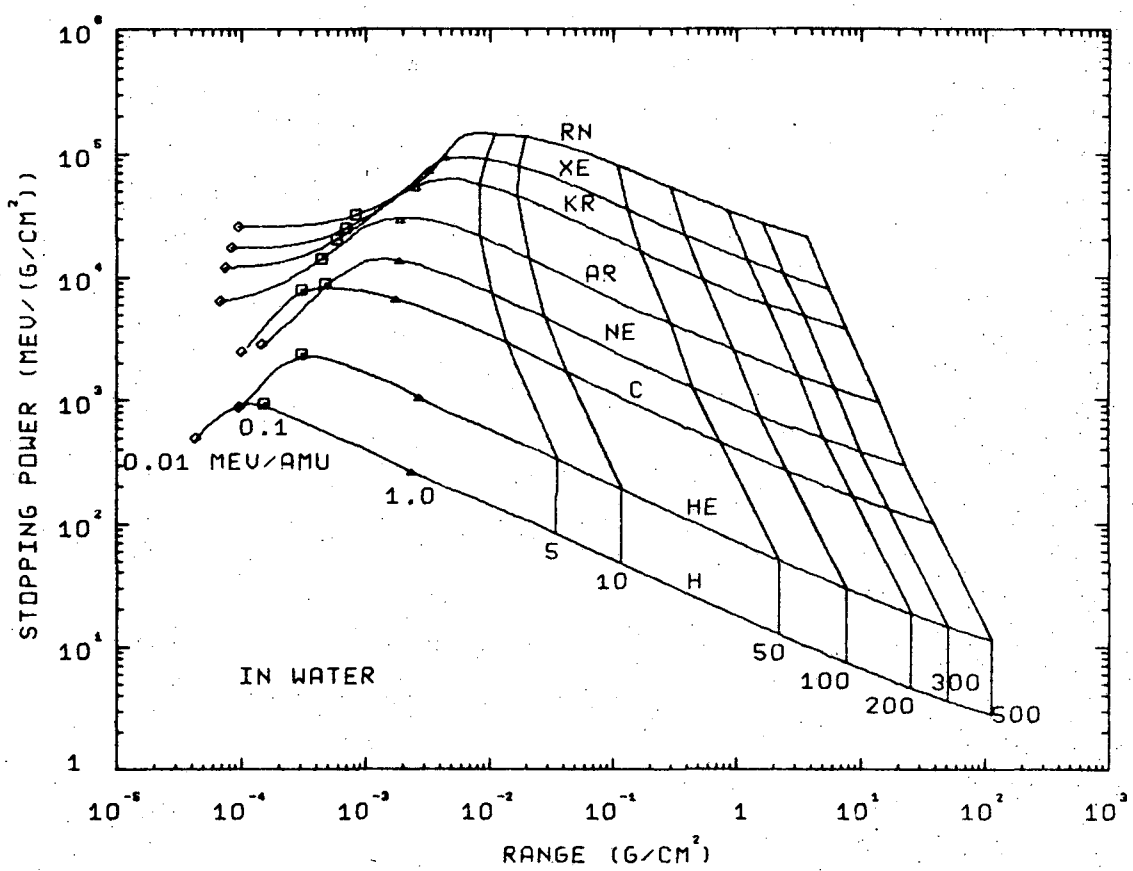

XBL 685-827

Fig. 5. Stopping-power curves as a function of residual range for various ions in water as calculated by the computer program. Various ion specific energies in units of MeV/amu are designated on each curve by symbols for $\varepsilon \leq 1.0$ and by curves of constant velocity for $\varepsilon \geq 5$. The H-He, C-Ne, and Xe-Rn crossovers are discussed in the text.

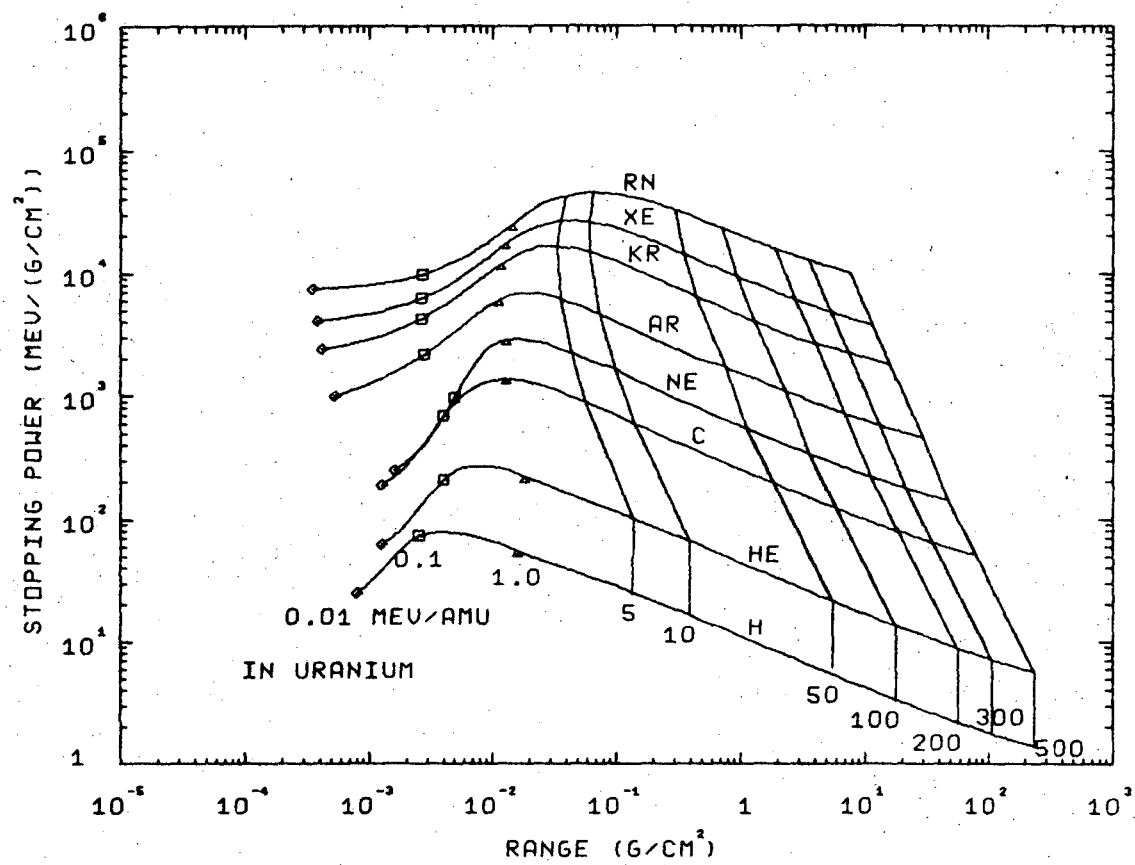

XBL 685-832

Fig. 6. Stopping-power curves as a function of residual range for various ions in uranium as calculated by the computer program. Various ion specific energies in units of MeV/amu are designated on each curve by symbols for $\varepsilon \leq 1.0$ and by curves of constant velocity for $\varepsilon \geq 5$.

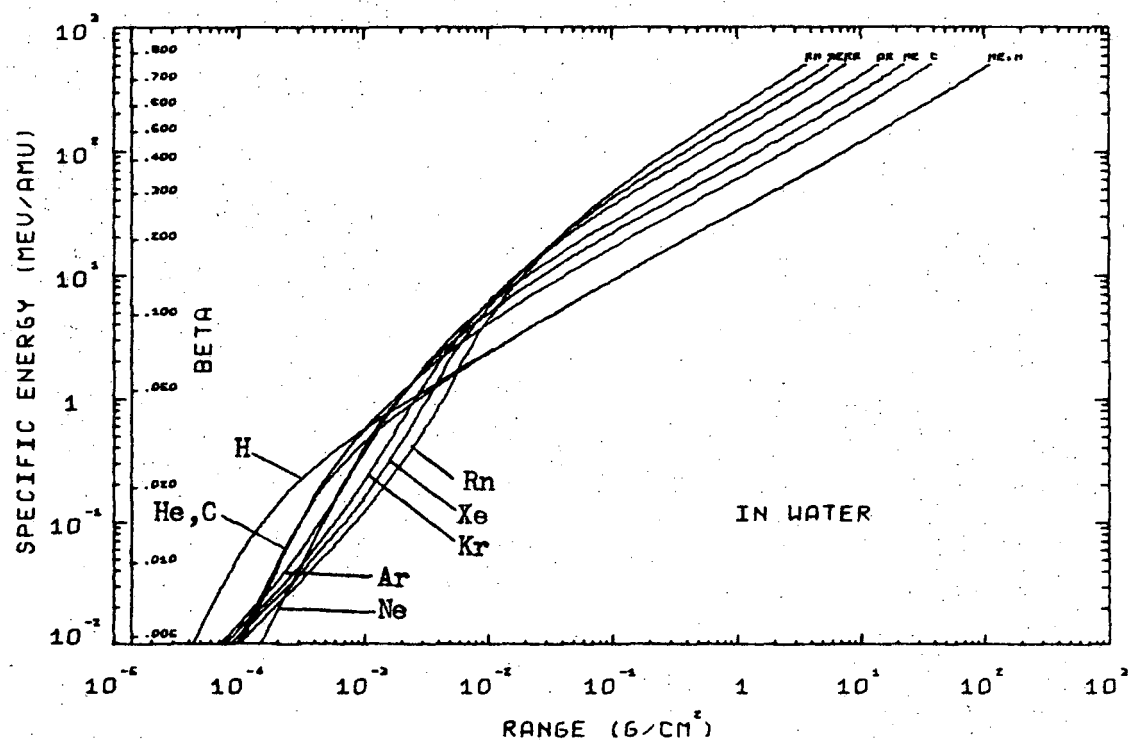

XBL 685-833

Fig. 7. Energy-range curves for various ions in water as calculated by the computer program. For any specific energy on the ordinate, the residual pathlength range is read from the abscissa. At the left of the figure, values of $\beta = V/c$ are displayed.

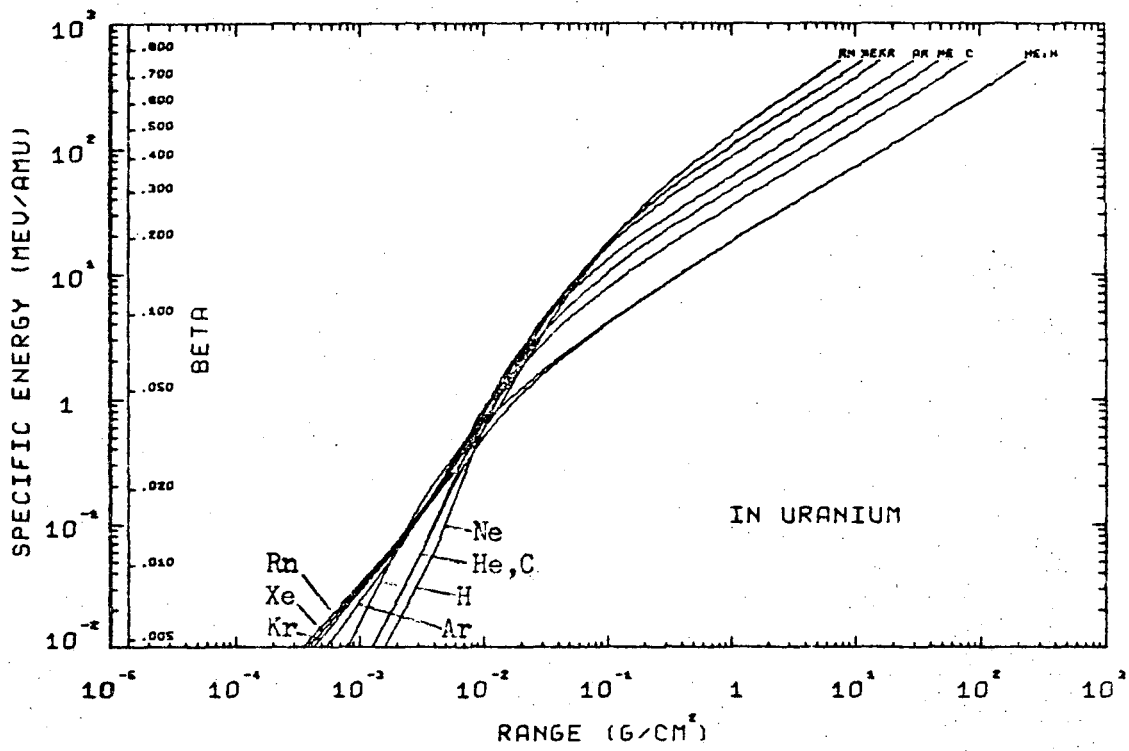

XBL 685-838

Fig. 8. Energy-range curves for various ions in uranium as calculated by the computer program. For any specific energy on the ordinate, the residual pathlength range is read from the abscissa. At the left of the figure, values of $\beta = V/c$ are displayed.

Part I

NOTATION

Symbol	Description of Symbol
ε	The specific energy of the ion in units of MeV per atomic mass unit of the ion.
Z_1	The atomic number of the ion (projectile).
Z_2	The atomic number of the stopping medium (target).
β	The ratio of the velocity of the ion to that of light in a vacuum.
A_1	Atomic weight of the ion.
V	The velocity of the ion.
E	Energy of the ion in units of MeV.
r	The ratio of the root mean square of the ion Z_1 to that of its nucleus.
m	The mass of the ion.
$\frac{dE}{dR}$	Stopping power in units of MeV/(g/cm^2).
c	The velocity of light.

Part II. Bragg Peaks, Flux and Spectra

1. Introduction

We will now consider a beam of monoenergetic particles incident on a slab of material whose transverse dimensions are large compared with the beam dimensions and with the depth of penetration of the beam. As these particles traverse the medium they lose energy through a variety of processes, the predominant ones being ionization energy loss, nuclear interactions, and small-angle multiple scattering. Other processes, including large-angle Coulomb scattering and elastic nuclear scattering, are usually of secondary importance when the initial energy of the beam particles is significantly greater than a few MeV per amu.

The energy loss of a beam of ions results primarily from many collisions between the beam ions and the electrons of the medium, causing a net transfer of energy to the medium. This process is referred to as ionization energy loss.

There are many facets to the highly complex process of charge exchange and ionization energy loss, but a wealth of experimental evidence backs up a great deal of theoretical work. Consequently, very good estimates are available for the rate of ionization energy loss of many ions in many different materials. The state of knowledge with regard to heavy-ion ionization energy loss has been summarized by Northcliffe.[10]

At very high particle energies, nuclear reactions can play an important role in the energy-loss process. A great many different reactions occur, and the total process is exceedingly complex. In some of the collision processes, many different secondary particles can be produced, and each of these gives up energy to the medium by the processes of ionization loss (charged particles only) and nuclear interaction (all particles).

The total cross section for nuclear interactions is known reasonably well over most energies of interest in this work. From this, attenuation factors can be calculated for the beam particles at all penetration distances.

Although the effect of nuclear attenuation on the flux, dose, and spectral curves is taken into account, the additional terms due to the secondary particles produced by the nuclear interactions are neglected in this work.

Elastic scattering of the beam ions by the nuclei of the target causes a small fraction of the total energy deposition in certain regions of the ion energy, in the form of kinetic energy of the recoil target nuclei. This effect is included as a correction term in the calculation of the total stopping power.

In addition to this elastic process, both the incident ion and the target nucleus can be raised to an excited state during an interaction in which the two bodies do not actually merge to produce a single compound nucleus. This effect is commonly referred to as Coulomb excitation, and as a result of such an interaction, each of the two bodies may be raised as high as an MeV or two above its respective ground state. For the energies of interest in this work, the contribution from Coulomb excitation to the total stopping power is negligible.

The process of small-angle multiple scattering leads to a divergence of the beam. As a result, the mean range of the particles decreases somewhat, and the range distribution is broadened. The basic scattering law is well known, so that it is possible to make reasonably accurate estimates of the multiple-scattering effects.

The process of ionization-energy loss occurs in discrete steps, rather than being continuous. This process leads to the general concept of straggling, whereby a given particle energy does not correspond to a unique distance of travel. Instead, for a given distance of travel, there is a distribution of particle energies, and for a given particle energy, there is a distribution of distances of travel. This distance distribution is of paramount importance in calculating Bragg curves.

Various other processes which are not important influence the passage of charged particles through matter; they include large-angle Rutherford scattering, energy transport via fast secondary electrons (gamma rays), and Cerenkov radiation.

The classical method of calculating Bragg curves is described by Evans.[14] This simple method is based on the assumption that the processes of nuclear attenuation and multiple scattering can be neglected, and that only range

straggling need be considered. Although useful for low-energy beams, this method is of little utility for the work described here; for the beams of interest here, both nuclear interactions and multiple scattering must be considered.

Complete details of these calculations are given by Litton et al.[15]

2. Theory

A. Number Density

We first consider the problem of deriving an expression which describes the attenuation of a beam of particles as they traverse a medium. The beam particles are all assumed to have an initial energy E_o, to be perfectly collimated, and to strike the surface of the medium in a direction parallel to the surface normal. The medium is assumed to be homogeneous, with transverse dimensions large compared both with the beam dimensions and with the depth of penetration of the beam particles.

The medium is assumed to be characterized by a total nuclear-reaction macroscopic cross section $\Sigma(E)$ (in cm^{-1}) and by a stopping power, or specific energy loss, $f(E)$ (in $MeV\text{-}cm^2/g$).

The path of the beam particles is characterized by the dimension $\bar{s}(E)$, which is defined as the mean distance traveled by particles which have gone from an initial energy E_o to an energy E. Consider those particles that have reached an energy E, denoted by the function $N_e(E)$. In traversing an incremental distance Δs, these particles lose on the average an energy (per amu!) ΔE. Since $f(E)$ is the total energy lost by each particle in a unit distance of travel, then the relation between ΔE and Δs is

$$\Delta E/\Delta s = f(E)/A_p \ , \tag{10}$$

where A_p is the atomic weight of the beam particles.

For this group of particles, the fractional decrease in their numbers in going from E to E-ΔE is given by the macroscopic reaction cross section multiplied by the mean distance traveled in losing this energy. Thus, we have

$$\frac{\Delta N_e}{N_e}(E) \approx -\Sigma(E)\cdot\Delta s. \tag{11}$$

Using Eqs. 10 and 11 we obtain

$$\frac{dN_e}{N_e}(E) = A_p \cdot \frac{\Sigma(E)}{f(E)}\, dE, \tag{12}$$

where we have taken the limit as ΔE tends to zero.

Equation 12 thus gives the fractional decrease in the number of particles in losing the increment of energy dE.

Integration of Eq. 12 yields the number density of a given energy within the slab,

$$N_e(E) = N_o(E_o)\cdot\exp\{-A_p\int_E^{E_o} [\Sigma(E'/f(E')]dE'\}, \tag{13}$$

where $N_o(E_o)$ is the number of incident particles, all of which have an energy E_o.

1. Mean Path Length of Travel

A very good approximation to the mean path length traveled by particles that have gone from energy E_o to energy E is obtained by direct integration of Eq. 10:

$$\bar{s}(E) = A_p\int_E^{E_o}[1/f(E')]dE'. \tag{14}$$

2. A Limiting Case

If the reaction cross section is energy-independent, it may be removed from under the integral sign in Eq. 13. Then, we have

$$N_e(E) = N_o(E_o)\cdot\exp\{-A_p\Sigma\int_E^{E_o}[1/f(E')]dE'\}.$$

By using Eq. 14 this becomes simply

$$N_e(E) = N_o(E_o)\cdot\exp\{-\Sigma\cdot\bar{s}(E)\},$$

which is a well-known result.

B. Path-Length Distribution

To obtain an expression for the energy deposition and for the flux at a particular distance of travel s, we must relate the energy of an ion to its position. This is done by defining a path-length distribution function as follows.

For a group of particles, each with energy E, $M(s,\bar{s})ds$ is the fraction of these particles that have traveled a distance s, where $\bar{s}$ is the mean distance traveled by particles of energy E_o and is given by Eq. 14.

Lewis[16] has shown that if the path-length distribution is a result of statistical fluctuations in the energy-loss process, then the distribution function should be well represented by a Gaussian.

Therefore, the path-length distribution function is written in the form

$$M(s,\bar{s}) = \frac{1}{\sqrt{2\pi}\ \sigma(E,E_o)} \cdot \exp\left\{ - \left[\frac{s - \bar{s}}{\sqrt{2}\ \sigma(E,E_o)} \right]^2 \right\} ds. \tag{15}$$

The quantity $[\sigma(E,E_o)]^2$ is the variance in the path-length distribution for particles slowing down from energy E_o to energy E.

Note that there may be a small range of energies near E_o for which Eq. 15 does not hold. Thus, consider an energy E near E_o. If $\sigma(E,E_o)$ is not sufficiently large, then the distribution function cannot be symmetric, because s can never be less than zero (no path length).

Thus, for Eq.15 to be valid, we require that E be small enough so that the inequality

$$\bar{s}(E) \gg \sqrt{2}\ \sigma(E,E_o)$$

is satisfied.

Many authors have adopted the convention of using the quantity called the straggling parameter, equal to $\sqrt{2}\ \sigma(E,E_o)$, rather than the standard deviation $\sigma(E,E_o)$.

We now transform the distribution $M(s,\bar{s})$ as follows. Defining the variable U as

$$U(E) = \frac{s - \bar{s}(E)}{\sqrt{2}\ \sigma(E,E_o)}, \tag{16}$$

we can write

$$M(s,\bar{s})ds = M(U)\ dU = \frac{1}{\sqrt{\pi}}\ e^{-U^2}\ dU. \tag{17}$$

The distribution M(U)dU may now be interpreted as the fraction of particles of energy E that have traveled a distance s such that the normalized difference between s and the mean distance of travel $\bar{s}(E)$ is

within an increment dU of U, and U is the normalized difference given by Eq. 16 Therefore, given the total number of particles $N_e(E)$, as calculated from Eq. 13 the number of those having traveled a distance s is given as

$$dN(s,E) = N_e(E)\cdot M(U)dU, \tag{18}$$

where U is an implicit function of E and is given by Eq. 16.

C. Flux and Dose Distributions

The total flux at a distance s is now obtained by integration of Eq. 18 from $U(E_o)$ to $U(0)$. Using Eqs. 13 and 17 and changing the variable of integration from U to E, we obtain the total flux at a distance s:

$$N(s) = N_o(E_o)\int_o^{E_o} \exp\left\{-A_p\int_E^{E_o} \frac{\Sigma(E')}{f(E')}\,dE'\right\}\left[\frac{e^{-U^2}}{\sqrt{\pi}}\right]\left(\frac{dU}{dE}\right) dE\ . \tag{19}$$

The mean range of the particles, $R(E_o)$, is given by Eq. 14 with E = 0. The quantity $\sigma^2(E_o)$ is the variance for particles having come to rest. It is equivalent to $\sigma^2(E,E_o)$ with E = 0; that is

$$\sigma^2(E_o) \equiv \sigma^2(0,E_o).$$

We also wish to calculate the total dose at s. If dN(s) represents a certain number of particles of energy E, as given by Eq. 18, then dN(s)f(E) is the dose per unit distance of travel of these particles at s. Thus, the total dose is

$$D(s) = \int_{\text{All } E} dN(s,E)\ f(E).$$

Using Eqs. 13, 17, and 18 we then have

$$D(s) = N_o(E_o)\int_o^{E_o} \exp\left\{-A_p\int_E^{E_o} \frac{\Sigma(E')}{f(E')}\,dE'\right\}\left[e^{-U^2}\right]\frac{f(E)}{\sqrt{\pi}}\,(dU/dE)dE \tag{20}$$

It should be noted that in Eqs. 19 and 20 the independent variable E appears, as well as the variable U. In order to perform the integration, one of these must be expressed in terms of the other. This is easily done, inasmuch as the unique relationship between them is given by Eq. 16.

D. Energy Spectrum

At any given position s, the total flux may be written as

$$N(s) = \int_{\text{All } E} N(E,s)\ dE,$$

where $N(E,s)dE$ is the number of particles having energies within dE of E. Comparing this expression with that given by Eq. 19, we deduce that the spectrum at any position is given as

$$N(E,s) = N_o(E_o) \exp\left\{-A_p \int_E^{E_o} \frac{\Sigma(E')}{f(E')} dE'\right\} e^{-U^2} \cdot \frac{1}{\sqrt{\pi}} (dU/dE),$$

with U given by Eq. 16.

E. Some Simplifying Cases

Suppose that the cross section is independent of energy. Then, as before, we may remove Σ from beneath the integral in both Eqs. 19 and 20. When Eq. 14 is used, the expressions for the flux and the dose simplify to

$$N(s) = N_o(E_o) \int_o^{E_o} \exp\{-[\Sigma\bar{s}(E) + U^2]\} \frac{(dU/dE)}{\sqrt{\pi}} dE \tag{21}$$

and

$$D(s) = N_o(E_o) \int_o^{E_o} \exp\{-[\Sigma\bar{s}(E) + U^2]\} \frac{f(E)}{\sqrt{\pi}} (dU/dE)dE \tag{22}$$

The integrals in both Eqs. 21 and 22 must be evaluated numerically.

A further simplification is obtained in the limiting case, where the attenuation due to nuclear interactions is negligible, as it would be for ions of sufficiently low energy. In that case, the cross section is assumed to go to zero, and the expressions for the flux and the dose reduce to

$$N(s) = N_o(E_o) \int_o^{E_o} e^{-U^2} \frac{(dU/dE)}{\sqrt{\pi}} dE \tag{23}$$

and

$$D(s) = N_o(E_o) \int_o^{E_o} e^{-U^2} \cdot f(E) \frac{(dU/dE)}{\sqrt{\pi}} dE.$$

The latter expression for the flux is equivalent to the classical expression, derived by Evans[14] and others. It can be obtained from basic principles as follows.

We assume that the distribution of ranges for particles with initial energy E_o is Gaussian, with a variance $[\sigma(E_o)]^2$:

$$P(R) = \frac{1}{\sqrt{2\pi}\,\sigma(E_o)} \exp\left\{-\left[\frac{R-R(E_o)}{\sqrt{2}\,\sigma(E_o)}\right]^2\right\},$$

where $R(E_o)$ is the mean range. The flux at a given distance s is contributed to by all particles whose range is greater than s. If the initial flux is $N_o(E_o)$ at s = 0, then the flux at s is given as

$$N(s) = N_o(E_o) \int_s^\infty \frac{1}{\sqrt{2\pi}\ \sigma(E_o)} \exp\left\{ - \left[\frac{R-R(E_o)}{\sqrt{2}\ \sigma(E_o)} \right]^2 \right\} dR \tag{24}$$

If we change variables from R to W, where W is given as

$$W = \frac{R-R(E_o)}{\sqrt{2}\ \sigma(E_o)} ,$$

Eq.24 becomes

$$N(s) = N_o(E_o) \int_{\frac{s-R(E_o)}{\sqrt{2}\ \sigma(E_o)}}^\infty e^{-W^2} \frac{dW}{\sqrt{\pi}} ,$$

which is equivalent to Eq. 23.

F. Nuclear Interactions

Energy deposition from nuclear interactions arises from two sources -- direct and indirect. The direct contribution comes from the deexcitation of the compound nucleus formed by the interaction of the target atom with the bombarding ion. A certain fraction of this deexcitation energy is released at the point of impact, and it is this fraction which comprises the direct contribution. The indirect portion aroses from secondaries produced at points within the medium other than the position of interest.

1. Direct Contribution

The total number of interactions, per unit length of travel, of ions with energy E, due to those particles whose initial energy is E_o, is given by

$$r^o(E,s) = N(E,s)\ \Sigma(E).$$

The total energy release at s from the direct contribution is then

$$D_{dir}(s) = \int_o^{E_o} N(E,s)\ \Sigma(E)\ G(E)\ dE,$$

where G(E) is the energy deposited at s per nuclear interaction with a particle of energy E.

2. Indirect Contribution

Let $H(E',s' \rightarrow s)$ be the energy released at s due to a nuclear interaction

of an ion of energy E' at s'. Then the total indirect contribution to the linear energy transfer, denoted $D_n(s)$, is given by

$$D_n(s) = \int ds' \int dE' N(E',s')\Sigma(E')\ H(E',s' \rightarrow s). \tag{25}$$

The simple form of Eq. 25 belies the inherent difficulties involved with its evaluation; although, as will be indicated, N(E,s) can be calculated, the function $\Sigma(E)$ is usually not well known. Furthermore, even less is known about the function $H(E',s' \rightarrow s)$.

For the work in this report, we neglect the contributions to the dose and flux from secondary particles.

G. Variance of the Path-Length Distribution

1. Energy-Loss Fluctuations

The process of ionization-energy loss occurs in a random fashion, so that one expects that, over a finite energy interval, the path-length distribution of particles with given energy will be Gaussian.

Suppose that a particle has an energy E_{tot}. From Lewis,[16] the average number of collisions experienced by the particle per unit distance of travel, in which an energy loss T occurs, is given by the expression

$$N_T(T)\ dT = \frac{k\ dT}{2\ E_{tot}\ T^2}, \tag{26}$$

where constant k is given as

$$k = 2\pi\ n_e\ Z_p^2\ M_p\ e^4/m_e,$$

and where n_e is the number of electrons per unit volume of the target and M_p and Z_p are the mass and atomic number of the incident particle. The

function $N_T(T)$ is often referred to as the collision spectrum.

Now, in traversing an increment of distance Δs, the average number of collisions in which an energy loss T occurs is given by

$$N_T(T)\, dT\Big|_{\Delta s} = \frac{k\, dT}{2\, E_{tot}\, T^2}\, \Delta s.$$

Since the collisions occur randomly, the standard deviation associated with the average number $N_T(T)dT$ is equal to the square root of that number. The variance $\langle N_c^{\,2}\rangle$ in the number of collisions is therefore equal to

$$\langle N_c^{\,2}\rangle = \frac{k\, dT}{2\, E_{tot}\, T^2}\, \Delta s.$$

Because each collision is associated with an energy loss T, the variance in the total energy loss over the distance Δs is given as

$$\langle \delta\, E_{tot}^2\rangle = T^2\, \langle N_c^{\,2}\rangle = \frac{k\, dT}{2\, E_{tot}} \cdot \Delta s. \tag{27}$$

For each value of T, there is a corresponding variance given by Eq. 27. Inasmuch as the collisions associated with each value of T are independent, the variances for all values of T are additive. Therefore, the net variance in the total energy loss associated with an incremental distance Δs is given by the sum

$$\langle \Delta\, E_{tot}^2\rangle = \sum_{\text{All } T} \frac{k\, dT}{2\, E_{tot}}\, \Delta s,$$

and in the limit, by

$$\langle \Delta\, E_{tot}^2\rangle = k \int_{T_{MIN}}^{T_{MAX}} \frac{dT}{2\, E_{tot}}\, \Delta s. \tag{28}$$

It can be shown that the maximum energy loss in a single collision is given by $\epsilon\, E_{tot}$, where

$$\epsilon = 4\, m_e/[M_p(1 + m_e/M_p)^2]. \tag{29}$$

A discussion of the lower limit is given by Bloch, who shows that it

can usually be neglected.[17] Integrating Eq. 28 using Eq. 29 we have

$$\langle \Delta E_{tot}^2 \rangle = \frac{4\pi n_e Z_p^2 e^4}{(1+m_e/M_p)^2} \Delta s. \tag{30}$$

Equation 30 gives the variance in the energy loss produced by collisions in Δs.

Evans[14] gives an argument to show that the relationship between an energy variance and the corresponding variance in the path-length distribution is given as

$$\langle \Delta R^2 \rangle = \frac{1}{[f(E)]^2} \langle \Delta E_{tot}^2 \rangle, \tag{31}$$

where E_{tot} is the mean energy of the particles in question.

Substituting the expression given by Eq. 30 into Eq. 31 we obtain

$$\langle \Delta R^2 \rangle = \frac{4\pi n_e Z_p^2 e^4}{(1+m_e/M_p)^2} \cdot \frac{\Delta s}{[f(E)]^2},$$

which is the contribution to the variance in the path length due to collisions in Δs. Since collisions within each increment Δs are independent from those in any other increment, the net variance over a group Δs_i will be the sum of the individual variances. As the Δs_i approaches zero, the sum becomes an integral, and we obtain

$$\langle \Delta R^2 \rangle = \frac{4\pi n_e Z_p^2 e^4}{(1+m_e/M_p)^2} \int_{E_1}^{E_2} \frac{ds}{[f(E)]^2} .$$

Using Eq. 10, we have

$$\langle \Delta R^2 \rangle = \frac{4\pi n_e Z_p^2 e^4}{(1+m_e/M_p)^2} A_p \int_{E_1}^{E_2} \frac{dE}{[f(E)]^3} . \tag{32}$$

This is the expression for the contribution to the variance in the path-length distribution for particles going from an energy E_2 to an energy E_1.

The final expression for the variance due to fluctuations in the ionization energy-loss process is therefore

$$\langle \Delta R^2 \rangle = \frac{1.3027 \times 10^{-25} n_e Z_p^2 A_p}{\rho} \int_E^{E_o} \frac{1 + H(E')}{H(E')} \frac{dE'}{[f(E')]^3} , \tag{33}$$

with the function H(E) given by $H(E) = [M_o c^2/(E+M_o c^2)]^2$.

2. Initial Energy Spread of the Beam

The relationship between an energy interval ΔE_o and the corresponding distance of travel Δs_o is given by Eq. 10. If we interpret ΔE_o as the uncertainty in the initial energy, then the corresponding uncertainty in the path length is given as

$$\Delta s_o = A_p \frac{\Delta E_o}{f(E_o)}.$$

This is a constant uncertainty over the entire path length of the particles. The associated variance in the path-length distribution is therefore

$$\langle \Delta s_o^2 \rangle = \left[\frac{A_p}{f(E_o)} \right]^2 \langle \Delta E_o^2 \rangle .$$

Strictly speaking, a Gaussian distribution in the initial energy of the beam can lead to a Gaussian distribution in the path lengths only if f(E) is constant over the energy range of the distribution.

3. Multiple-Scattering Contributions

As a charged particle travels through a medium, it undergoes what is commonly termed small-angle multiple scattering. This arises principally from electromagnetic interactions between the charged particle and the nucleus.

In order to arrive at expressions for the dose and flux in terms of the penetration distance x, we must convert from the distribution $M(s,\bar{s})$ to a distribution $M'(x,\bar{s})$. This is defined as the fraction of particles, all having slowed down to energy E from energy E_o, that are at a penetration distance x. To do this we proceed by calculating the mean square difference

between the path length s and the penetration distance x, as a function of s, denoted as $\langle (s-x)^2 \rangle$.

Referring to Fig. 9, we can deduce the relationship between a small change Δs in the distance of travel of a given particle, and the corresponding change Δx in the penetration distance,

$$\Delta x = \Delta s \cos \varphi,$$

where φ is the angle that the particle makes with the x direction. The change in the square of the difference $(s-x)^2$ is therefore given approximately as

$$\Delta(s - x)^2 = [\Delta s(1 - \cos \bar{\varphi})]^2,$$

where $\bar{\varphi}$ is the mean angle of the particles within ds. Again, making the assumption of independence of events, the net value of the mean square difference is given as the sum

$$\langle (s - x)^2 \rangle = \sum [(1 - \cos \bar{\varphi})\Delta s]^2. \tag{34}$$

We now proceed to the development of the penetration-distance distribution. For a given distance of travel, the distribution function of the difference (s - x) may be approximated by a Gaussian. The quantity $\langle (s - x)^2 \rangle$ given by Eq. 34 is then an estimate of the variance of this distribution. Since we are considering a particular value of s, then $\langle (s - x)^2 \rangle$ also represents the variance in the distribution of penetration distances corresponding to the distance of travel s.

Thus, if the distribution in (s - x) is given as

$$P(s - x) = \frac{1}{\sqrt{2\pi}} \exp \{-[(s - x) - D_o]^2/2\kappa^2\},$$

where the variance κ^2 is the mean square difference given by Eq. 34, and D_o is the mean about which the distribution is centered, then the distribution in penetration distances is

$$P(x) = \frac{1}{\sqrt{2\pi}} \exp \{-[x - \bar{x}]^2/2\sigma^2\}.$$

The quantity $\bar{x}$ is the mean value of the penetration distance, and is estimated simply as the difference between s and the mean difference between

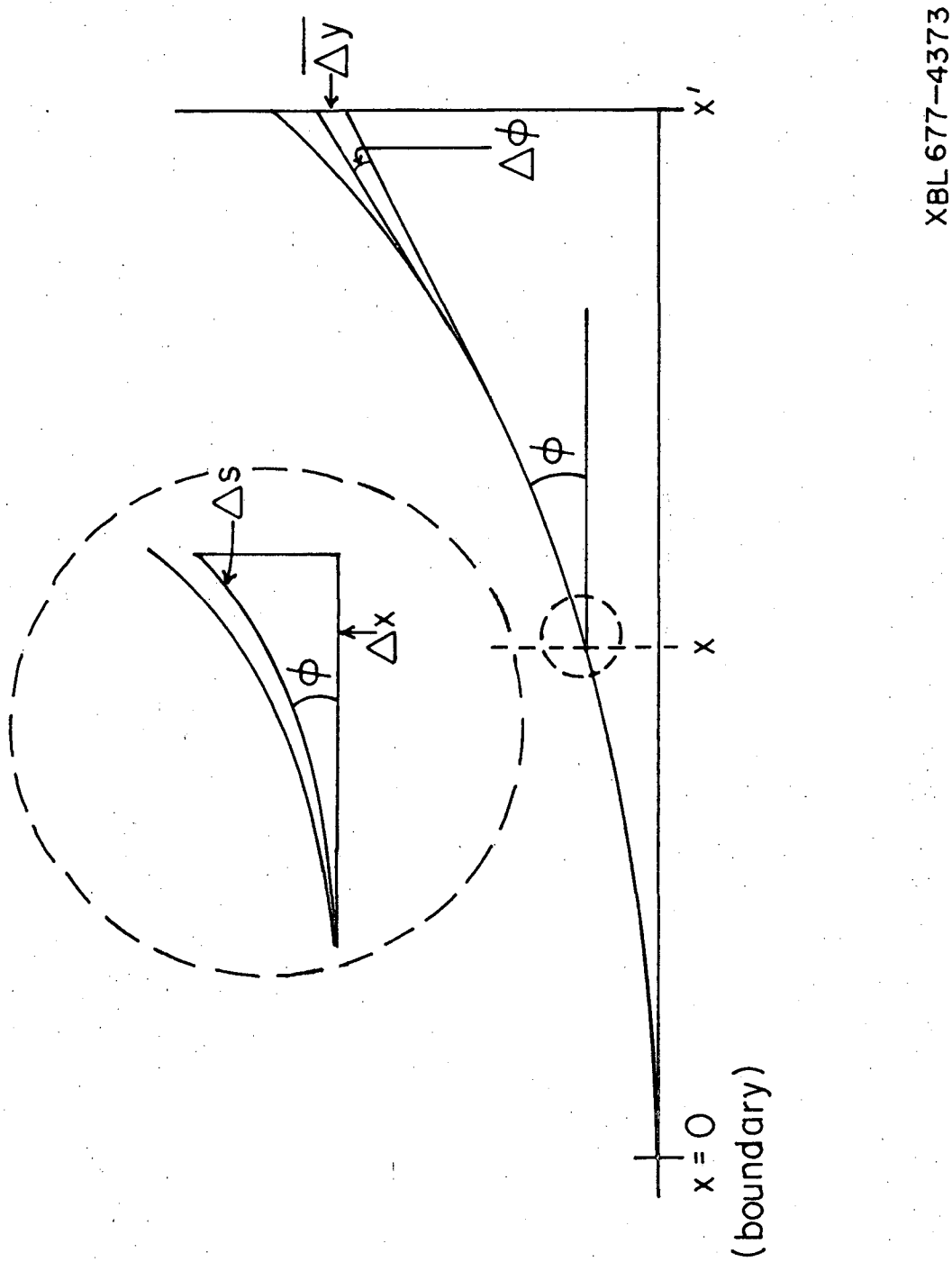

Fig. 9. Geometric model used in analyzing multiple-scattering effects.

s and x. Thus,

$$\bar{x} \approx s - \{\langle (s - x)^2 \rangle\}^{1/2}. \tag{35}$$

We may summarize as follows. For a given value of the energy E, the mean penetration distance is given by Eq. 35; the contribution to the variance in the penetration distance distribution from multiple scattering is given by Eq. 34.

H. Nuclear Reactions

For most of the cases of interest -- namely very heavy ions with energies on the order of a few hundred MeV per amu -- experimental data are essentially nonexistent; consequently, we must rely on theoretical considerations.

If we let R represent the radius of the geometric cross section, then at sufficiently high energies the microscopic cross section is given by

$$\eta = \pi R^2.$$

The radius of a nucleus may be expressed in the form

$$r = r_o \cdot A^{1/3} - SKT,$$

where A is the atomic weight of the nucleus, r_o is the nuclear unit radius, and SKT may be interpreted as an overlap parameter. Since the radius of the geometric cross section is simply the sum of the radii of the incoming particle and the target nucleus, we have

$$R = r_p + r_t, \tag{36}$$

where the subscripts "p" and "t" refer to the particle and target, respectively.

At low energies, the Coulomb barrier obviously plays a role in the interaction process. It can be shown[18] that if R, given in Eq. 36 in this

case, is the classical distance of closest approach, and V(R) represents the potential at this distance, then the cross section is given by

$$\eta = \pi R^2 \left[1 - \frac{V(R)}{E_{c.m.}}\right] \quad \text{for } E_{c.m.} > V(R), \text{ and}$$
$$\eta = 0 \quad \text{for } E_{c.m.} < V(R), \tag{37}$$

where $E_{c.m.}$ is the total energy of the particle in the center-of-mass system. The potential is given by

$$V(R) = \frac{Z_p Z_t e^2}{R}, \tag{38}$$

where Z_t is the nuclear charge. Equation 37 reflects the fact that classically the potential barrier cannot be crossed with less than a given amount of energy.

The exact form of the Coulomb correction is of secondary importance, since for almost all cases of interest in this study, $E_{c.m.}$ is much greater than V(R). Hence, the presence of the Coulomb barrier has almost no effect on the cross section for the energies of interest.

We must now consider the fact that the incoming particle exhibits wave properties, especially in the energy region where the equivalent wavelength is not trivially small. If the wavelength is denoted by $\lambda\!\!\!^{-}$, then the uncertainty in the position of the particle is also given by $\lambda\!\!\!^{-}$. Hence, one would expect that the "effective radius" of the particle-plus-target cross section would be enhanced by this amount. Thus, a better estimate of the cross section is

$$\eta = \pi(R + \lambda\!\!\!^{-})^2 \left[1 - \frac{V(R + \lambda\!\!\!^{-})}{E_{c.m.}}\right] .$$

At very high energies, $\lambda\!\!\!^{-}$ approaches zero and the cross section is given simply by πR^2. As the energy decreases, the cross section increases as the wave length becomes important. Finally, there is a sharp drop in the cross section near energies comparable to the potential threshold. Using Eqs. 36 and 38 we obtain the complete expression for the reaction cross section:

$$\eta = \pi[r_o(A_p^{1/3} + A_t^{1/3}) + \lambda\!\!\!^{-} - 2SKT]^2 \left[1 - \frac{Z_t Z_p e^2}{E_{c.m.}[r_o(A_t^{1/3} + A_t^{1/3} + \lambda\!\!\!^{-}]}\right] \tag{39}$$

It is convenient to express both the particle wavelength and center-of-mass total energy in terms of the laboratory energy E, in units of MeV per amu. These are given by the relationships

$$\lambda\!\!\!^{-} = \frac{\hbar c}{A_p(2E \cdot M_o c^2 + E^2)^{1/2}} \quad \text{and}$$

$$E_{c.m.} = \frac{A_p A_t}{A_p + A_t} E,$$

where $(M_o c^2)$ is the rest mass of an amu expressed in energy units (approx 931 MeV). Substituting numerical values, we obtain

$$\lambda\!\!\!^{-} = \frac{1.977 \times 10^{-11}}{A_p(1862\ E + E^2)^{1/2}} . \tag{40}$$

The Values of r_o and SKT

Most important in the use of Eq. 39 is the value of the nuclear unit radius r_o. In general, r_o varies somewhat from one nucleus to another; however, inasmuch as the concept of a nuclear radius is somewhat vague, it is permissible to use a single value of r_o for all nuclei.

Most earlier analyses of nuclear interactions have been made using a simpler model in which the parameter SKT was not considered. With this model, many attempts have been made to assign a value to r_o. Evans[14] has summarized the various methods utilized prior to 1955. These include:

a. Analysis of the β decay of certain isotopes to infer the value of the classical Coulomb-energy radius;

b. Quantum-mechanical corrections to the classical Coulomb-energy radius, leading to an equivalent electromagnetic radius;[19]

c. Analysis of isotopic shift in line spectra;[20]

d. Measurement of the characteristic electromagnetic radiations from μ-mesonic atoms;[19,21,22]

e. Analysis of fine-structure splitting of electronic x-ray levels in heavy atoms;[23]

f. Measurement of the lifetime of α ray emitters;[24]

g. Analysis of anomalous scattering of α particles;[23]

h. Measurement of the cross sections for nuclear reactions;[24]

i. Measurement of the elastic scattering of fast neutrons by nuclei.

By the use of several early works as guidelines, and by making use of the analysis of nuclear charge distribution by Hofstadter,[25] a set of values for r_o and SKT was found that fitted reasonably well the literature data. These values, 1.4 F for r_o and 0.4 F for SKT, were used in obtaining all the calculated results presented in this work.

1. Scattering Law

The quantity $P(\theta)d\theta$ is defined as the number of collisions per unit distance of travel of a particle, which deflect the trajectory of the particle by an angle which is within $d\theta$ of θ. The classical Rutherford scattering formula for this probability is given by Rossi[26] as

$$P(\theta)d\theta = \frac{1}{4} N_a Z_p^2 Z_t^2 r_e \cdot \frac{1}{A_t}\left(\frac{m_e c}{\beta p_{c.m.}}\right)^2 \cdot \frac{2\pi \sin\theta \, d\theta}{\sin^4(\theta/2)} , \tag{41}$$

where N_a is Avogadro's number, r_e is the classical electron radius, m_e is the electron mass, and $p_{c.m.}$ is the momentum of the particle. This equation applies to the c.m. system of coordinates; it may be valid in the lab system if the mass of the incident particle is much less than that of the atoms of the medium. Since for many cases of interest to this study this is not so, Eq. 41 must instead be considered in the c.m. system only.

For the purposes of this treatment, it will be convenient to leave the angle θ in the c.m. system, but to transform the momentum term into the lab system.

From the expressions derived by Halliday,[27] the relation between the momentum in the lab and c.m. systems is

$$p_{c.m.} = \left(\frac{1}{1+\gamma}\right) p_L , \tag{42}$$

where $\gamma = A_p/A_t$.

Using Eq. 42 in Eq. 41 and dropping the subscript on the lab momentum term, we have

$$P(\theta)d\theta = \frac{\pi}{2} \frac{N_a Z_p^2 Z_t^2}{A_t} r_e \left(\frac{m_e c}{\beta p}\right)^2 \frac{\sin\theta \, d\theta}{\sin^4(\theta/2)} (1+\gamma)^2 . \tag{43}$$

The limitations on the validity of Eq. 43 must be discussed. At extremely small angles, this equation fails because the electrons of the

scattering atom screen the particle from the field of the nucleus. Rossi[29] states that Eq. 43 is valid for angles significantly larger than $\lambda\!\!\!^{-}/r_a$, where $\lambda\!\!\!^{-}$ is the de Broglie wavelength of the incident particle divided by 2π and r_a is the radius of the atom; whereas, for angles less than $\lambda\!\!\!^{-}/r_a$, Eq. 43 grossly overestimates the scattering probability. In fact, one can see that the equation is singular for $\theta = 0$.

Various attempts have been made to modify Eq. 43 in order to take into account the screening effect. Using an atomic potential of the form $V = (Z_t Z_p e^2/r) \exp(-r/r_a)$, Goudsmit and Saunderson[28,29] show that the scattering-probability law takes the form

$$P(\theta)d\theta = \frac{8\pi N_a Z_p^2 Z_t^2}{A_t} r_e \left(\frac{m_e c}{\beta p}\right)^2 \frac{\sin\theta\, d\theta}{[\theta^2+\theta_1^2]^2} (1+\gamma)^2 , \tag{44}$$

where

$$\theta_1 = \lambda\!\!\!^{-}/r_a . \tag{45}$$

By use of the expression in Eq. 40 and the classical expression for r_a,

$$r_a = \frac{1}{\alpha^2} r_e Z_t^{1/3} ,$$

with

$$\alpha = e^2/\hbar c ,$$

Eq. 45 is transformed to

$$\theta_1 = \frac{Z_t^{1/3}}{137} \frac{m_e c}{p} (1+\gamma) . \tag{46}$$

Note that θ_1 is in c.m., whereas p is the lab momentum.

Williams has derived corrections to the scattering law given in Eq. 44 for high energies, using a simple model for the charge distribution within the nucleus.[30] He shows that the fact that the charge is not concentrated in a single dimensionless point does not materially affect the scattering law for angles less than $\theta_2 \approx \lambda\!\!\!^{-}/r_n$, where r_n is an assumed radius for the nucleus. On the other hand, for $\theta > \lambda\!\!\!^{-}/r_n$, the scattering probability goes to zero much more rapidly than predicted by Eq. 43. Using for r_n the expression

$$r_n = 0.49\, r_e A_t^{1/3} ,$$

we can estimate an upper limit, θ_2, for nonzero values of the scattering probability:

$$\theta_2 \approx \frac{\lambda\!\!\!^{-}}{0.49\ r_e A_t^{1/3}} \cong 280\ A_t^{-1/3} \cdot \frac{m_e c}{p}\ (1 + \gamma). \tag{47}$$

It is convenient to express the various quantities appearing in Eqs. 44, 46 and 47 in energy rather than momentum units. To do this, we use the relativistic relation between momentum and energy,

$$p^2 = 2A_p^2 M_o E + A_p^2 E^2/c^2, \tag{48}$$

where E is in units of energy per amu, and M_o is the rest mass per amu.

The quantity β in terms of E is

$$\beta = \left[1 - \left(\frac{M_o c^2}{E + M_o c^2}\right)^2\right]^{1/2}. \tag{49}$$

Using Eqs. 48 and 49 in 44, 46, and 47, and rearranging terms, we obtain

$$P(\theta)d\theta = (8\pi N_a r_e^2)(m_e c^2)^2 \cdot \frac{1}{HH(E)} \frac{\sin\theta d\theta}{[\theta^2 + \theta_1^2]^2} \left(\frac{Z_p^2 Z_t^2}{A_p^2 \cdot A_t}\right) (1 + \gamma)^2 \tag{50}$$

with

$$HH(E) = \left[\frac{E(E + 2\ M_o c^2)}{E + M_o c^2}\right]^2 \tag{51}$$

$$\theta_1 = \frac{Z_t^{1/3}\ (1 + \gamma)}{137\ A_p} \frac{m_e c^2}{[E(E + 2M_o c^2]^{1/2}},$$

and

$$\theta_2 = \frac{280(1+\gamma)}{A_t^{1/3} \cdot A_p} \frac{m_e c^2}{[E(E + 2M_o c^2)]^{1/2}}.$$

If we substitute numerical values, these equations reduce to

$$P(\theta)d\theta = 0.3139 \left(\frac{Z_p^2 Z_t^2}{A_p^2 \cdot A_t}\right) (1 + \gamma)^2 \cdot \frac{1}{HH(E)} \frac{\sin\theta\ d\theta}{[\theta^2 + \theta_1^2]^2}, \tag{52}$$

with

$$HH(E) = \left[\frac{E(E + 1862)}{E + 931}\right]^2,$$

$$\theta_1 = 3.73 \times 10^{-3}\ \frac{Z_t^{-1/3}(1 + \gamma)}{A_p} \frac{1}{[E(E + 1862)]^{1/2}}, \tag{53}$$

and
$$\theta_2 = \frac{143.1\ (1 + \gamma)}{A_t^{1/3} \cdot A_p} \cdot \frac{1}{[E(E + 1862)]^{1/2}} \ . \tag{54}$$

2. Mean Square Angle of Deflection

We are now ready to calculate the mean square angle of deflection, denoted $\langle\varphi^2\rangle$, as a function of distance of travel. Since each scattering is independent and represents a very small fraction of the total scattering angle, the change in $\langle\varphi^2\rangle$ in a distance element Δs is

$$\Delta\langle\varphi^2\rangle \cong \Delta s \int \varphi_L^2 P_L(\varphi_L) d\varphi_L \ , \tag{55}$$

where φ_L is the scattering angle of a single collision (lab), and $P_L(\varphi_L)$ is the corresponding probability of occurrence per unit length. In the limit as $\Delta s \to 0$ we have

$$\frac{d}{ds} \langle\varphi^2\rangle = \int \varphi_L P_L(\varphi_L) d\varphi_L \equiv \varphi_s^2 \ , \tag{56}$$

where φ_s^2 is the mean square angle change per unit distance of travel.

Now, since all expressions describing the scattering process are in the c.m. system, we must transform Eq.56 as follows. Since there is a unique relation between an angle φ_L lab and the corresponding angle θ in the c.m. system, we may write

$$P_L(\varphi_L) d\varphi_L = P(\theta) d\theta .$$

Substituting into Eq. 56, then, we obtain

$$\varphi_s^2 = \int_{\theta_1}^{\theta_2} \varphi_L^2(\theta) P(\theta) d\theta, \tag{57}$$

where the functional dependence of φ_L on θ is indicated.

We now seek a simple means of relating φ_L to the c.m. angle. Halliday[30] has shown that this relationship is given by the expression

$$\tan \varphi_L = \frac{\sin \theta}{\cos \theta + \gamma} \ . \tag{58}$$

From an examination of the expression for θ_2 given by Eq. 54, we can conclude that for nearly all cases of interest, θ_2 is less than unity. Further, one can show that for those small energies for which θ_2 exceeds unity, the corresponding residual range of the ions is so small that the

multiple-scattering effects within that range are negligible. Therefore, we may replace Eq. 58 by the simpler expression

$$\varphi_L = \frac{\theta}{1 + \gamma} .$$

Substituting this expression for θ_L into Eq. 57 we obtain

$$\varphi_s^2 = \frac{1}{(1 + \gamma)^2} \int_{\theta_1}^{\theta_2} \theta^2 P(\theta) d\theta . \tag{59}$$

The integral in Eq. 59 is easily evaluated by using the expression for $P(\theta)$ given by Eq. 52. The result is

$$\varphi_s^2 = 0.15696 \frac{Z_p^2 Z_t^2}{A_p^2 \cdot A_t} \cdot \frac{1}{HH(E)} \left\{ \ln \left[\left(\frac{\theta_2}{\theta_1} \right)^2 + 1 \right] - \right\} 1 , \tag{60}$$

and θ_2/θ_1 is, from Eqs. 53 and 54,

$$(\theta_2/\theta_1) = \frac{3.836 \times 10^4}{(A_t Z_t)^{1/3}} , \tag{61}$$

and HH(E) is given by Eq. 51. Note that if θ_2 as calculated from Eq. 54 is greater than π, then the value of θ_2 is to be taken as π instead. In that case, the term θ_2/θ_1 is

$$\theta_2/\theta_1 = \frac{842.2 \cdot A_p [E(E + 1862)]^{1/2}}{Z_t^{1/3}(1 + \gamma)} . \tag{62}$$

Using these expressions for φ_s^2, we can proceed with the calculation of the mean square angle of deflection.

From Eq. 56, we have

$$\frac{d}{ds} \langle \varphi^2 \rangle = \varphi_s^2(E), \tag{63}$$

where we have indicated the dependence of φ_s^2 on the particle energy. This unique dependence on the energy is established by Eq. 60.

As an initial condition, we specify that

$$\langle \varphi^2 \rangle \Big|_{s=0} = \varphi_o^2 .$$

Integrating Eq. 63 then, from s = 0 to some value s, we have

$$\langle\varphi^2\rangle = \varphi_o^2 + \int_o^s \varphi_s^2(E')ds'$$

and

$$\langle\varphi^2\rangle = \varphi_o^2 + A_p\int_E^{E_o} \frac{dE'}{f(E')}\,\varphi_s^2(E').$$

For a perfectly collimated beam, φ_o is zero. However, if the initial beam has an angular distribution that can be represented by a Gaussian with some standard deviation, then φ_o is equal to this standard deviation.

The mean angle of deflection $\bar{\varphi}$ is estimated to be the square root of the mean square angle. Thus we write

$$\bar{\varphi} = [\langle\varphi^2\rangle]^{1/2}.$$

3. Scattering for Multiple Materials

The difficulty involved in treating a target composed of more than one type of atom is that there is no unique relationship between the c.m. and lab systems. That is, for each type of target atom, there is a different c.m. system. Consequently, it is necessary to resort to further approximations in order to arrive at results that are applicable in the lab system. The method used is as follows.

The scattering probability function given by Eq. 50 is rewritten

$$P(\theta)d\theta = \left(\frac{N_a\rho}{A_t}\right)\left\{8\pi r_e^2\cdot(m_e c^2)\cdot \frac{1}{HH(E)}\cdot \frac{\sin\theta\, d\theta}{[\theta^2+\theta_1^2]^2}\left(\frac{Z_p Z_t}{A_p}\right)^2 (1+\gamma)^2\right\}\frac{1}{\rho},$$

where $(N_a\rho/A)$ is the number of atoms of the scatterer per cubic centimeter, and ρ is the total density of the scattering medium. The term in the braces is then interpreted as the probability of scattering into $d\theta(\theta)$ per atom of scattering material.

The scattering probability for scattering atom type "i" is hence

$$P_i(\theta)d\theta = \frac{8\pi N_i}{\rho}\,(r_e\cdot m_e c^2)^2\cdot\left[\frac{Z_p Z_i(1+\gamma_i)}{A_p}\right]^2\cdot\frac{1}{HH(E)}\,\frac{\sin\theta\, d\theta}{[\theta^2+\theta_1^2]^2};$$

where N_i is the number of type "i" atoms per cubic centimeter, and ρ is the total density of the medium.

The mean square angle change per unit distance, due to type "i" atoms,

is then

$$(\varphi_s^2)_i = 2.606 \times 10^{-25} \left(\frac{N_i}{\rho}\right) \left[\frac{Z_p Z_i}{A_p}\right]^2 \cdot \frac{1}{HH(E)} \left\{ \ln\left[\left(\frac{\theta_2}{\theta_1}\right)^2 + 1\right] - 1 \right\},$$

where the results embodied in Eq. 60 have been used. Also, by use of Eqs. 61 and 62, we have

$$\left(\frac{\theta_2}{\theta_1}\right)_i = \frac{3.836 \times 10^4}{(A_i Z_i)^{1/3}} \qquad \text{for } \theta_2 < \pi$$

and

$$\left(\frac{\theta_2}{\theta_1}\right)_i = 842.2 \frac{A_p [E(E + 1862)]^{1/2}}{Z_i^{1/3}(1 + \gamma_i)} \quad \text{for } \theta_2 \geq \pi.$$

We now consider the problem of obtaining an estimate of the net mean square scattering angle. Equation 56 may be written as

$$\frac{d}{ds} \langle \varphi^2 \rangle = \sum_i \int \varphi_L^2 P_i(\varphi_L) d\varphi_L = \Sigma(\varphi_s^2)_i \ , \tag{64}$$

where the $P_i(\varphi_L)$ are the probabilities due to the various scattering species.

The mean square angle at s is then obtained, as before, by integration of Eq. 64 from s = 0 to s.

4. Multiple-Scattering Effects

Earlier, it was shown that the scattering process leads to a contribution to the variance in the path-length distribution. Other effects that can be calculated from the equations describing the scattering are discussed below.

a. Radial Spreading

Of particular interest is the function $\langle y^2 \rangle$, which is defined as the mean square distance of travel in a direction perpendicular to the initial direction of travel, and is a function of the mean distance of travel s. For simplicity, it is denoted as the mean square radial spread. This function characterizes the general shape of the beam within the medium, and can be used to estimate the minimum beam size necessary to ensure against excessive effects due to spreading.

Suppose the mean-square beam spread at some positions in the medium is given as $\langle y^2 \rangle$. Clearly, then, if the initial dimensions of the beam are much greater than $[\langle y^2 \rangle]^{1/2}$, the effect of radial spreading will be small.

That is, the fractional change in the beam dimensions will be much less than unity.

On the other hand, if the beam radius, say, is much smaller than the value of $\langle y^2 \rangle$ at some distance s, then the beam at that point will have smeared out to the extent that the shapes of the flux and dose curves are grossly altered from what they would be for a large-diameter beam.

We proceed to the calculation of the function $\langle y^2 \rangle$. Referring to Fig. 9, we can express the change in the mean-square radial spread at x' due to a change in the mean angle of deflection φ at some $x < x'$. Thus, we have

$$\Delta y \equiv [\Delta\langle y^2 \rangle]^{1/2} = (x' - x)\Delta\varphi \ ,$$

so that

$$\Delta\langle y^2 \rangle = (x' - x)^2 \ \Delta\langle \varphi^2 \rangle \ . \tag{65}$$

The change in the mean square angle is given by Eq. 55 and substituting into Eq. 65 we have

$$\Delta y^2 = (x' - x)^2 \cdot \varphi_s^2 \ \Delta s \ . \tag{66}$$

Recognizing that the contributions to the mean square radial spread are additive, we obtain

$$\langle y^2 \rangle = A_p \int_E^{E_o} (x - x')^2 \varphi_s^2 \frac{dE'}{f(E')} + (\Delta y_o)^2 \ , \tag{67}$$

where we have interchanged the variables x and x' for convenience. The quantity $(\Delta y_o)^2$ is the contribution to the radial spread variance at x due to an initial angular spread of the beam particles. Thus, if φ_o is the initial mean angle of the beam particles, then reference to Fig. 9 and Eq. 66 shows that $(\Delta y_o)^2$ is

$$(\Delta y_o)^2 = x^2 \varphi_o^2 \ ,$$

where $(\Delta y_o)^2$ is evaluated at a penetration distance x.

It is shown later that, in many cases, the term $(\Delta y_o)^2$ dominates the right-hand side of Eq. 67, even for quite small values for φ_o. In other words, the mean beam deflection can be a strong function of the initial angular spread. Numerical examples are presented in the section dealing with results.

The variable x' is related to the energy E' through the expressions in Eqs. 35 and 14.

Equation 67 thus gives an expression for the variance in the radial spread distribution for particles having reached an energy E. We may define a mean beam deflection as the square root of $\langle y^2 \rangle$. This is another measure of the amount of radial spreading of the beam.

b. Beam-Spreading Attenuation

As the beam spreads, there may be an effective geometric attenuation of the flux and dose; i.e., the particles are spread out over a larger area. A very rough estimate of this effect is given as follows.

Let y_o be the radius of the initial beam. At some penetration distance x, suppose that the mean-square radial spread is $\langle y^2 \rangle$. Then at that point, one can say that the beam "effective radius" is estimated to be $y_o + y$, where y is the mean beam deflection. Therefore, the attenuation factor will be simply

$$f = \left(\frac{y_o}{y_o + y}\right)^2 = \left(\frac{1}{1 + y/y_o}\right)^2 . \tag{68}$$

As the ratio y/y_o increases, one would expect this function to more nearly represent the attenuation of the center-line flux and dose.

For the experimental situation in which the sensitive-area dimensions of a detector are much larger than the maximum value of y, there is no attenuation of the form given by Eq.68 . Similarly, if the beam were very broad and the diameter of the sensitive area of the detector were small, no attenuation would result. On the other hand, the function f would be expected to give the proper attenuation for the situation in which (i) the ratio y/y_o is large, and (ii) the counter diameter is small compared with y_o.

c. Range Shortening

Because the particles follow curved paths, the effective range in the medium is somewhat less than if the particles all traveled in straight lines. If R is the effective range of the particles and S_R is the corresponding mean distance of travel, then Eq. 35 gives their relationship as

$$R = S_R - \langle s - x \rangle \Big|_R , \tag{69}$$

where $\langle s - x \rangle \big|_R$ is the mean difference at the range.

The choice of definition of the range is somewhat arbitrary, and several are in common usage. For the purposes of evaluating the expression in Eq. 69, the value chosen for the range is immaterial, since $\langle s - x \rangle$ is

virtually constant in the vicinity of the end of the range. That this is so follows from the fact that when the mean angle of deflection becomes significant, the mean energy is so low that the residual range is a minute fraction of the total range. That is, although the particles are traveling at large oblique angles, their remaining distance of travel is so small that the contributions to $\langle s - x \rangle|_R$ are negligible.

The degree of range shortening is often expressed in terms of a quantity called the percentage detour factor, which is defined by Berger and Seltzer[31] as

$$D = \frac{100 \langle s - x \rangle|_R}{S_R} .$$

IV. RESULTS

Presented in this section are the results of calculations based on the analyses presented in the preceding sections. For the most part, these calculations were performed by using the program BRAGG,[32] which was written to solve the various equations developed in this work.

A. Bragg, Flux, and Spectral Curves for Monoenergetic Beams

In this section, results are presented for the case in which the initial beam of particles is assumed to be perfectly collimated (zero angular spread) and to be monoenergetic. In later sections, the effects due to finite energy and angular spreads are discussed.

In a discussion of Bragg curves, there are two quantities of particular interest. One is the ratio of the dose at the peak to that at the incident surface, denoted as the peak-to-plateau ratio. The other is the width of the Bragg peak, measured at those two points at which the dose is equal to one-half the dose at the peak. This is called the full width at half maximum, which we shall abbreviate to the "peak width" for convenience.

Also of considerable importance is the shape of the spectrum at the Bragg peak. Of particular interest are the average energy at the peak and the full width at half maximum.

We consider first the case in which the target material is water. Figure 10 shows the Bragg curves for various ions in water, with the Bragg peak at 5.0 g/cm^2. Figure 11 shows the flux curves for the same ions and Fig. 12 shows the spectra at the peak. Also, the peak-to-plateau ratio and the Bragg peak width are plotted as functions of the atomic number of the beam in Figs. 13 and 14.

As shown by these figures, the peak-to-plateau dose ratio reaches a maximum value for a value of the beam atomic number between 6 and 8. Beyond a value of 10, the dose ratio falls off monotonically.

On the other hand, the peak width falls off extremely rapidly with increasing atomic number, up to a value of approximately 20. For greater values of atomic number the width increases quite slowly. This behavior can in part be explained by considering the effective charge of the ions as they traverse the medium.

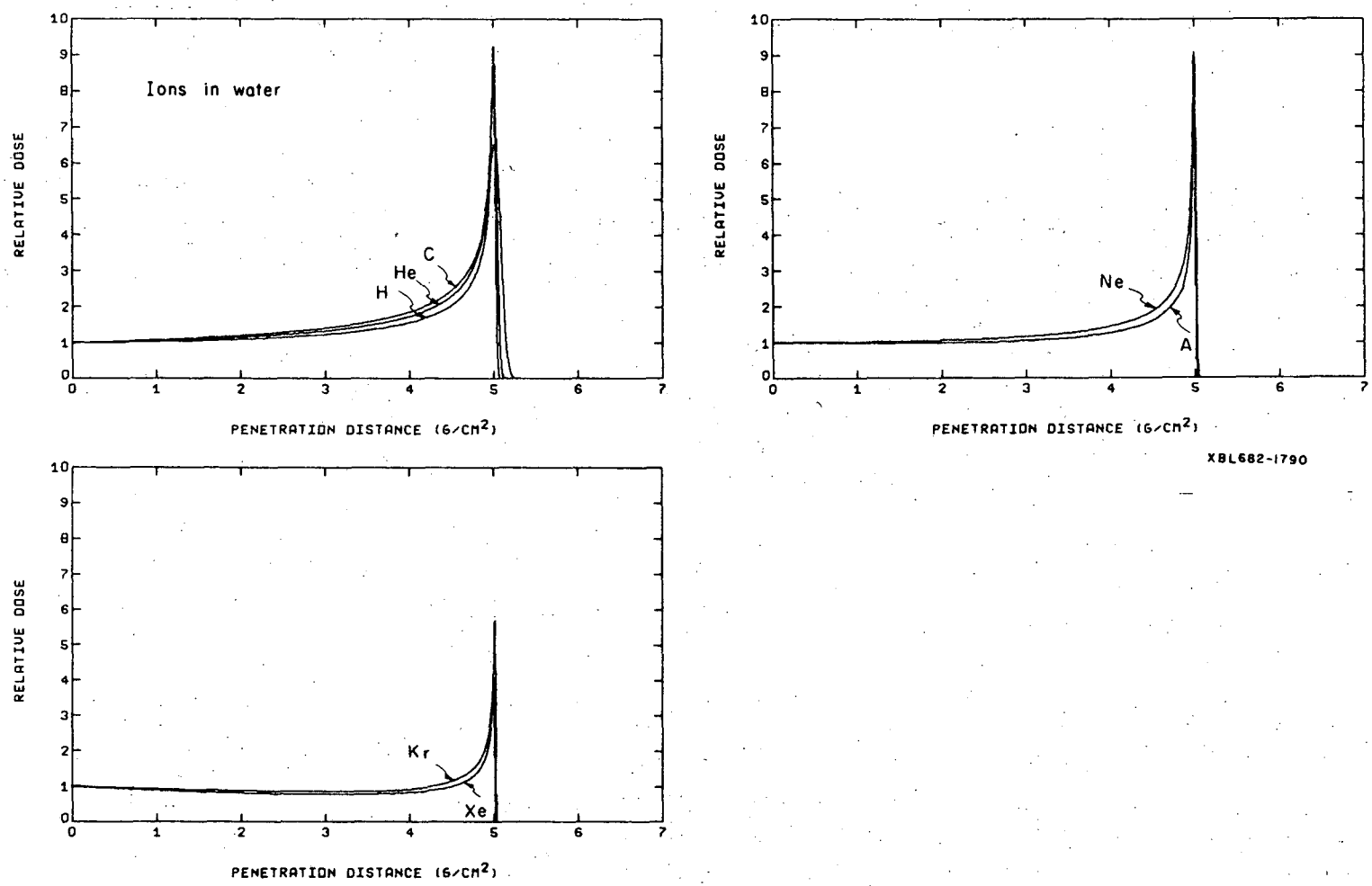

Fig.10. Bragg curves for ions in water, with the peak at 5 g/cm^2: (a) H, He, and C; (b) Ne and A; (c) Kr and Xe.

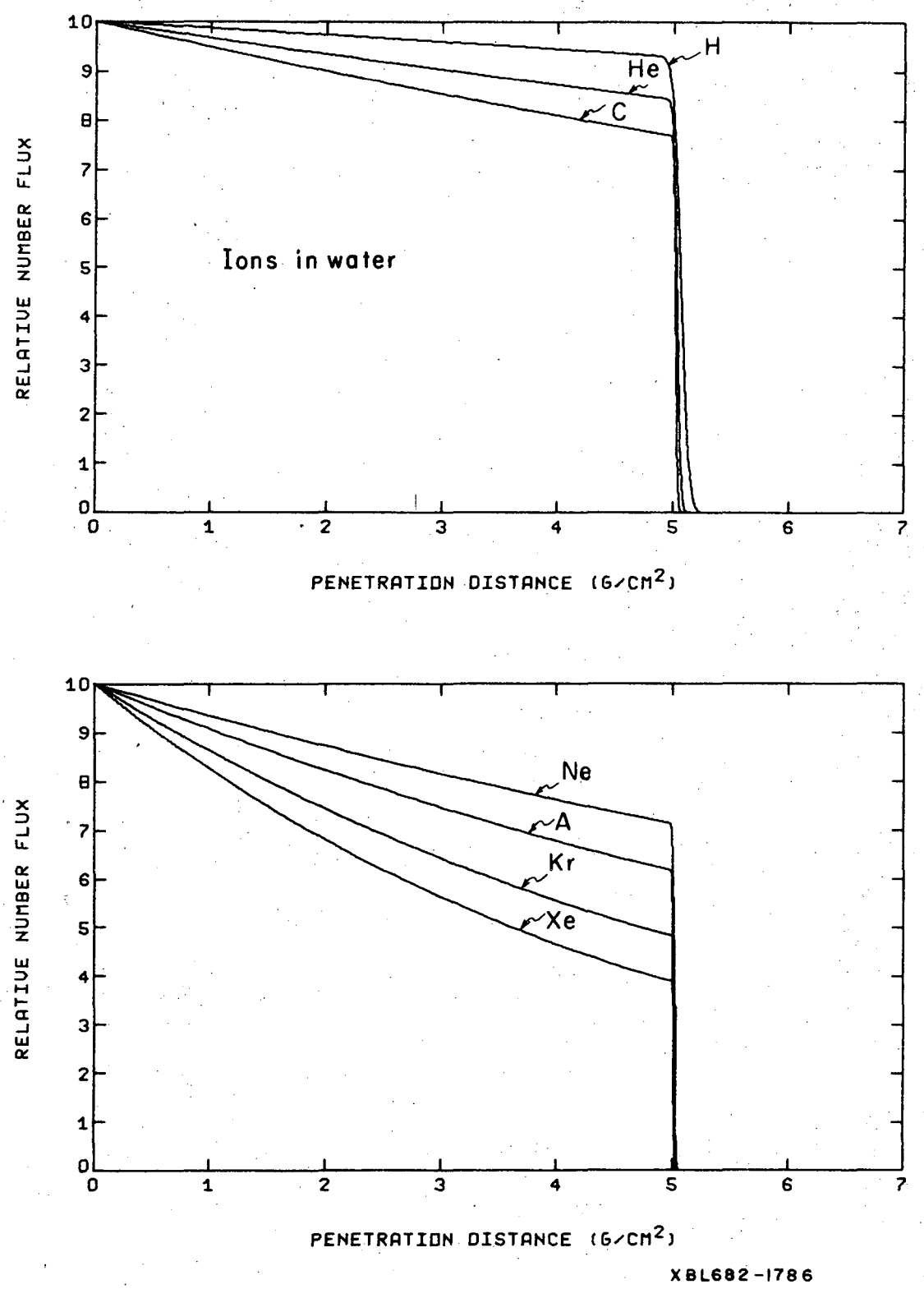

Fig. 11. Flux curves for ions in water with the peak at 5 g/cm^2: (a) H, He, and C; (b) Ne, A, Kr, and Xe.

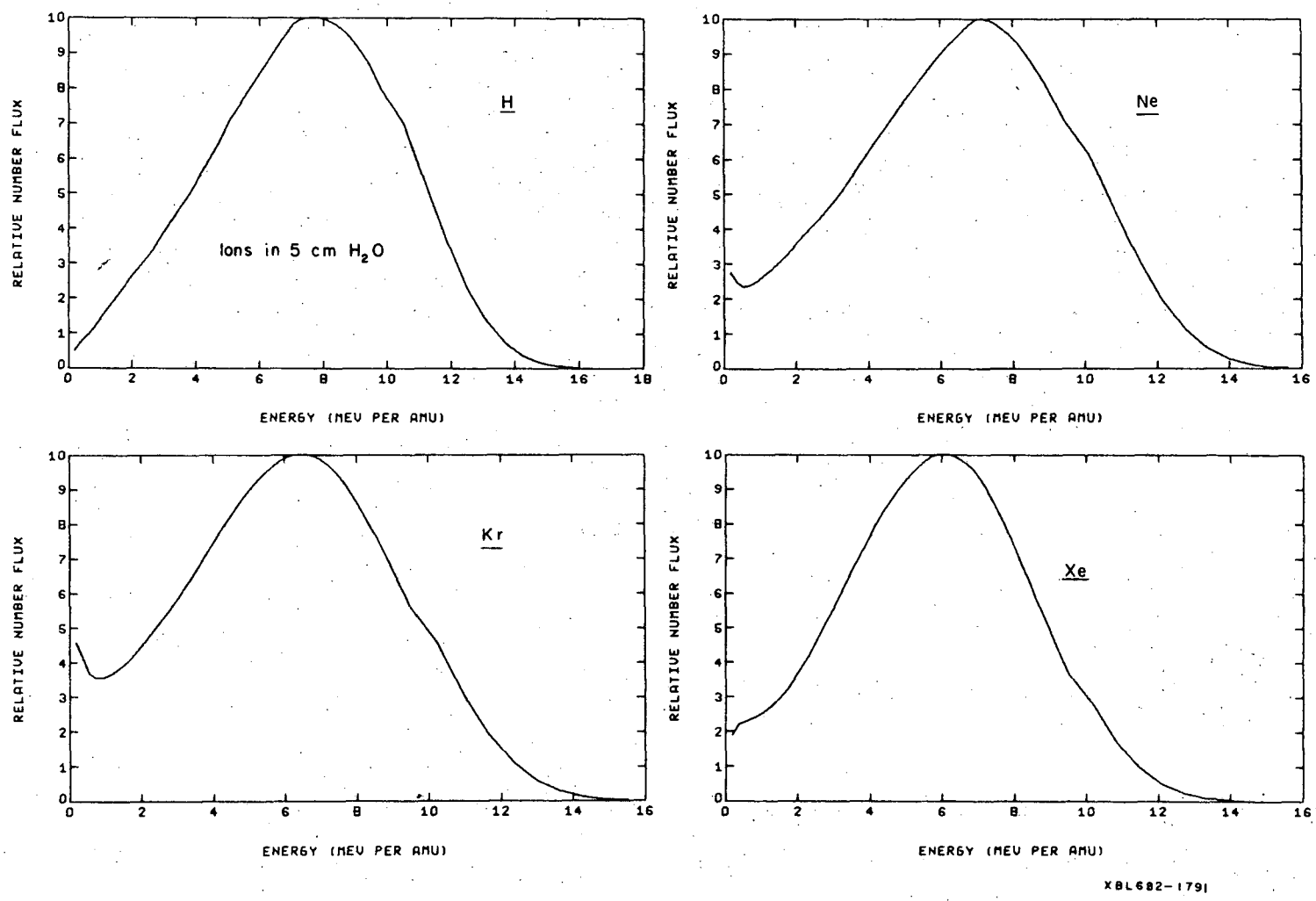

Fig. 12. Spectra at the Bragg peak for ions in water, with the peak at 5 g/cm^2: (a) protons; (b) neon; (c) krypton; (d) xenon.

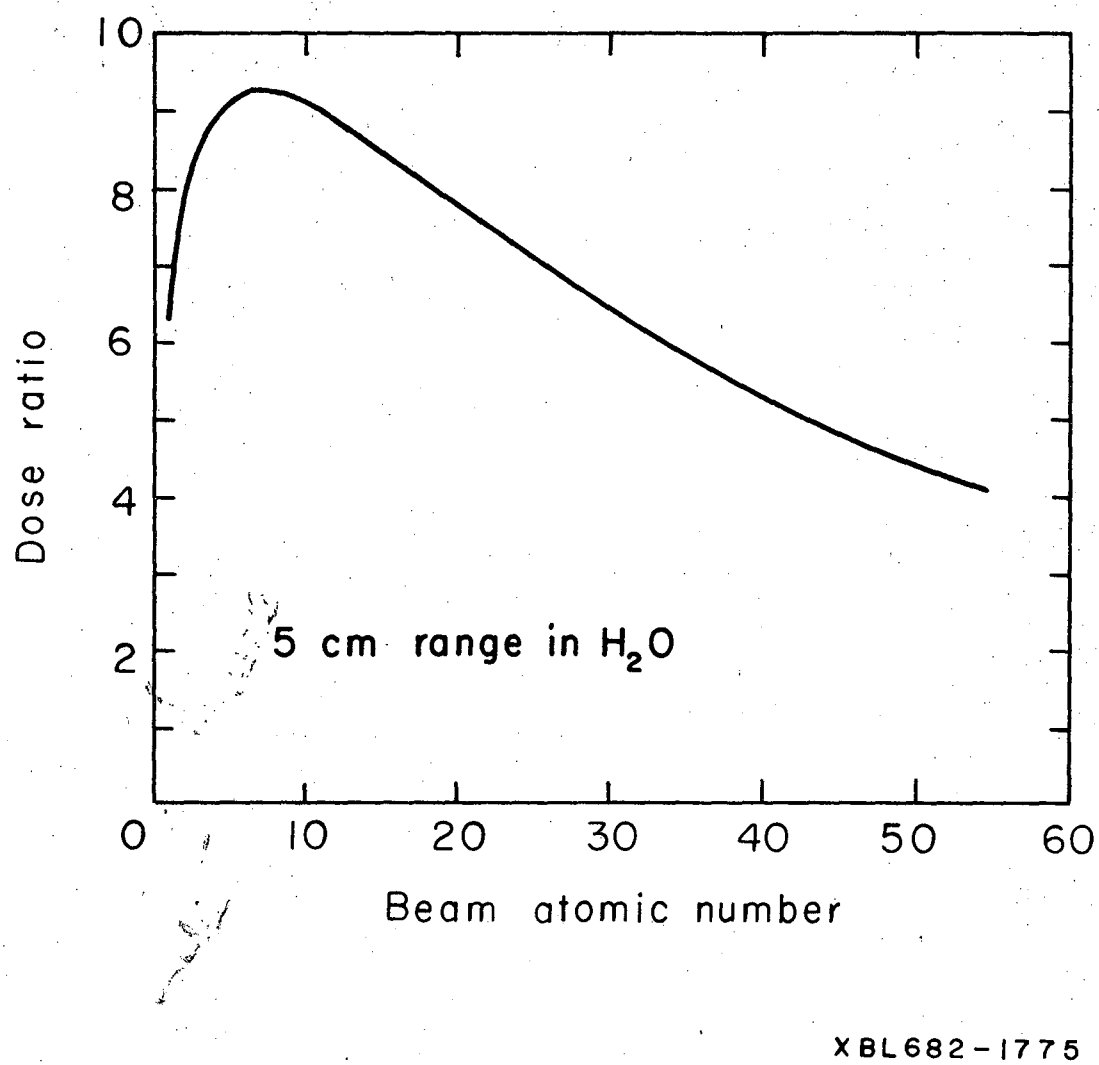

Fig. 13. Peak-to-plateau dose ratio for ions in water, with the peak at 5 g/cm^2.

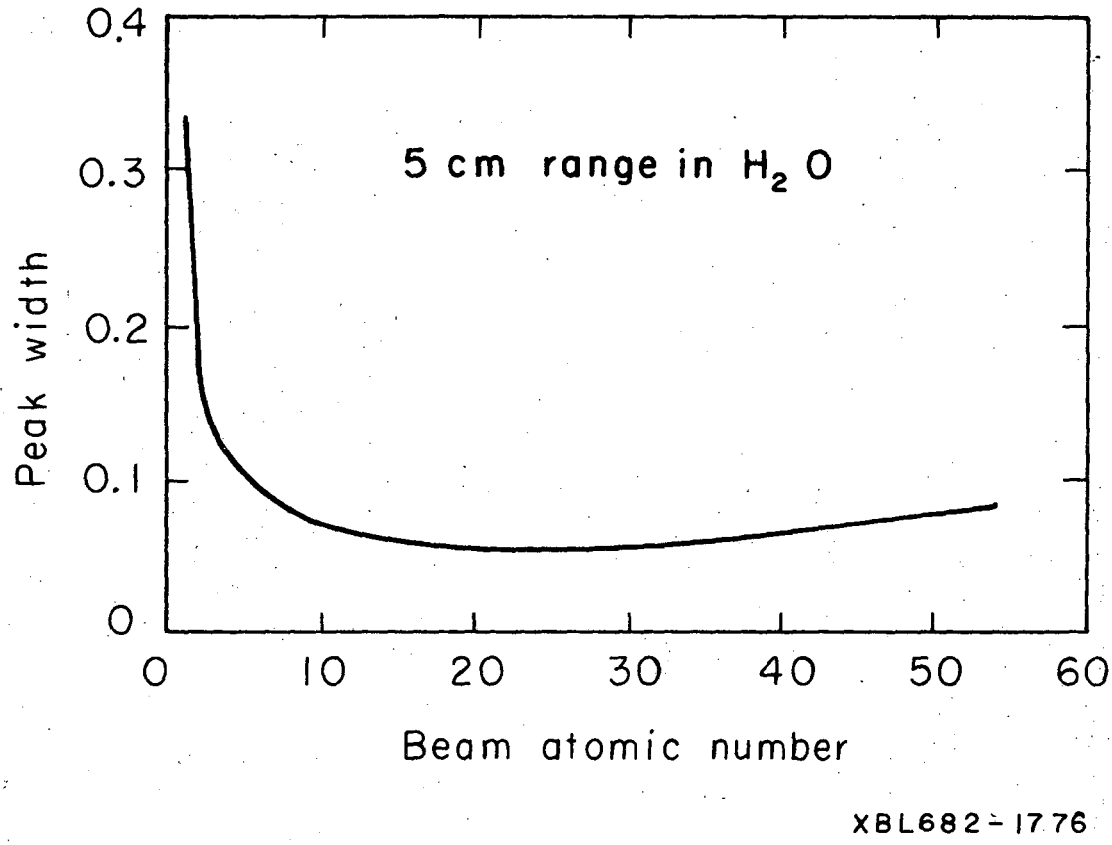

Fig. 14. Bragg peak width for ions in water, with the peak at 5 g/cm^2.

Effect of Different Energies

Suppose one wishes to produce Bragg peaks at various penetration depths within a given medium, using a given ion. It would be useful to be able to predict the changes in the various features of the physical process as functions of the depth at which the peak is produced, or alternatively, as functions of the initial beam energy. This section presents results that depict these functional dependences.

We consider two separate systems: protons incident on a water target, and neon ions incident on a water target. These cases serve to demonstrate the relationship between the initial beam energy and such quantities as the peak-to-plateau dose ratio and the Bragg peak width.

The results for the two systems are embodied in Figs. 15 through 18 In general, the peak-to-plateau dose ratio goes through a maximum and then decreases monotonically with increasing energy. The peak width and peak average energy are increasing functions of the initial energy.

B. Consequences of Initial Energy and Angular Spreads

Actually, no beam can be perfectly collimated or monoenergetic. Generally, the energy distribution is approximately Gaussian and has a very narrow width. Also, as a result of many factors, there is a small angular distribution in the particles as they impinge upon the target. It will be shown that even very small widths in the initial energy and angular distributions can have strong influences on the shape of the Bragg and flux curves, and on the energy spectra.

We consider the case of protons and neon ions incident on water targets, with the Bragg peaks at 5 g/cm^2, and study the effects due to changes in the initial energy distribution. Figures 19, 20, and 21 show the Bragg, flux, and spectral curves for protons incident on water, for various values of the standard deviation in the initial energy distribution. Figures 22 and 23 show similar results for neon ions incident on water.

In general, these results show that a value for the standard deviation of less than 1 percent of the mean initial energy can alter the Bragg and spectral curves significantly. Consider the neon case as an example. An initial standard deviation of 0.5 MeV per amu, or approximately 0.25 percent

of the initial energy, produces a change in the peak-to-plateau ratio of approximately 25 percent, a change in the average energy at the peak of approximately 35 percent, and a change in the peak width of nearly 100 percent. Interestingly enough, there is very little effect on the shape of the flux curve for the given changes in the standard deviation.

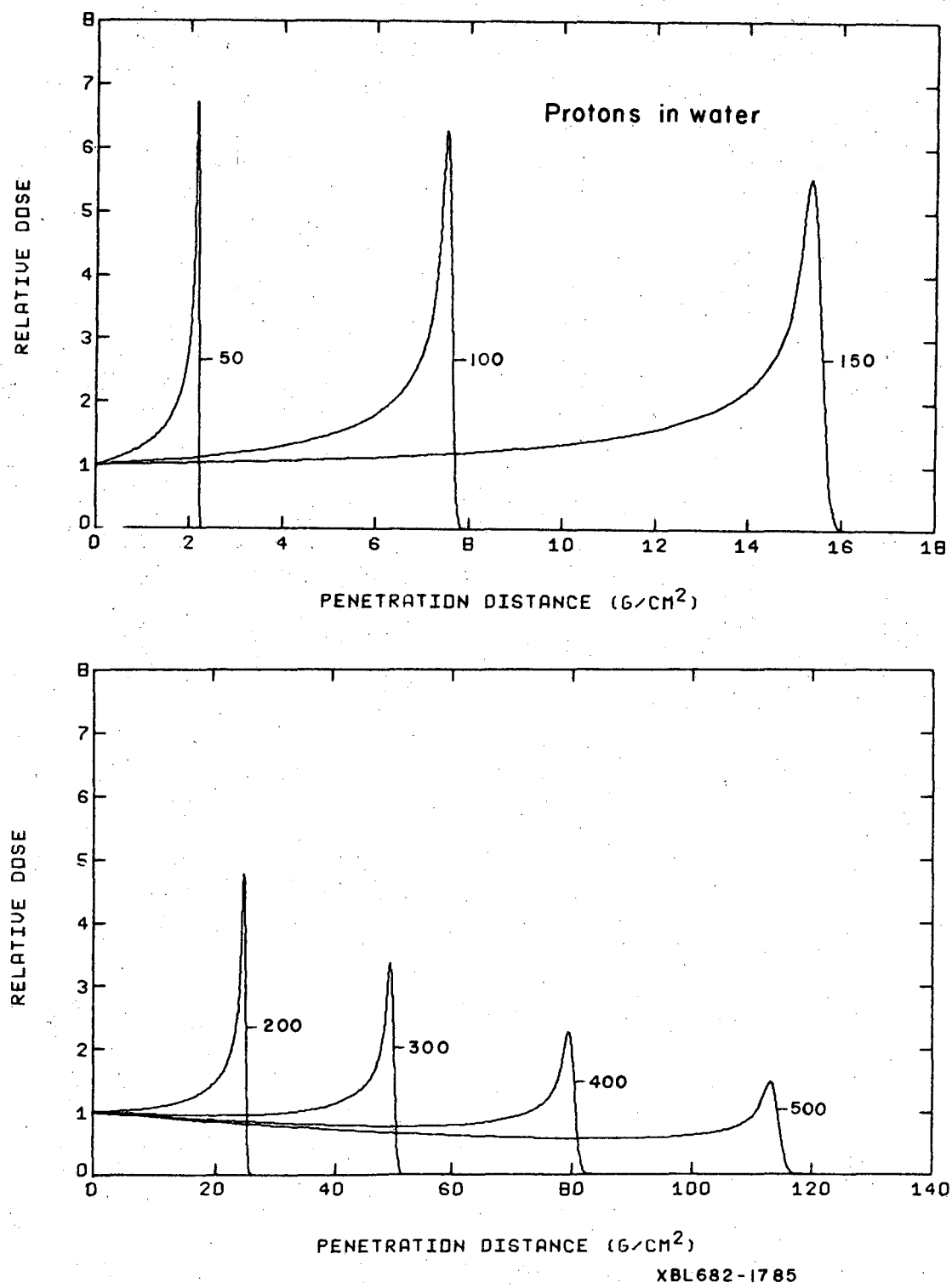

Fig. 15. Bragg curves in water for protons with initial energies ranging from 50 to 500 MeV.

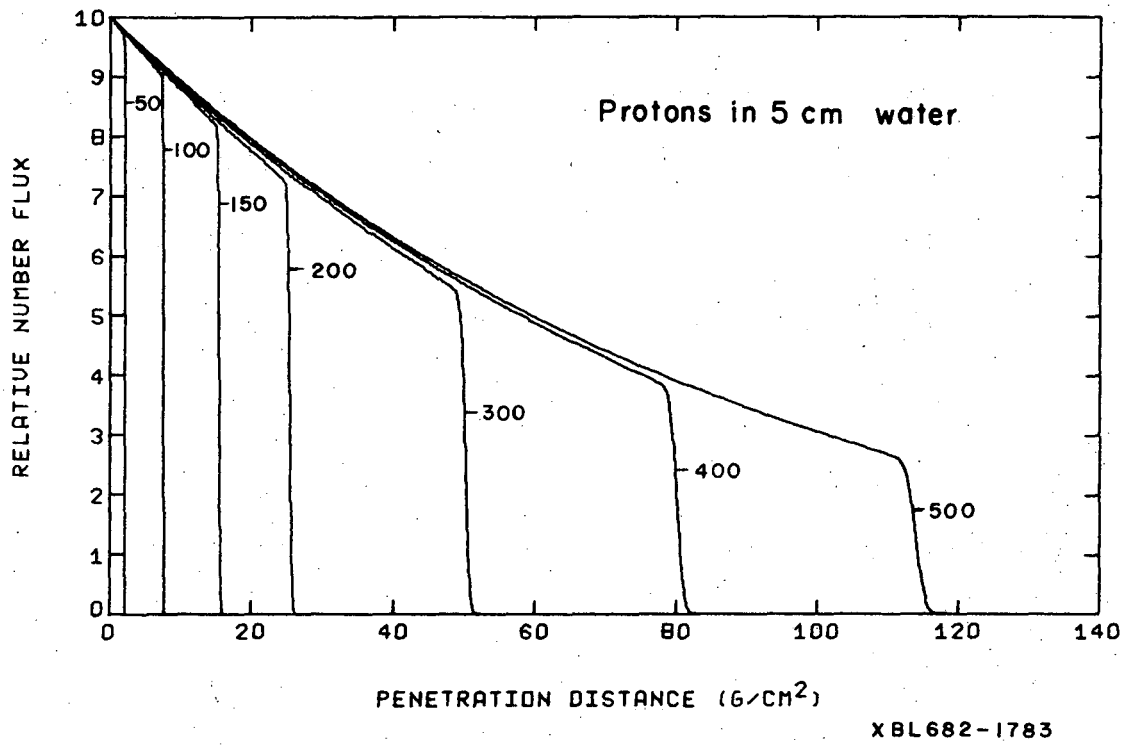

Fig. 16. Flux curves in water for protons with initial energies ranging from 50 to 500 MeV.

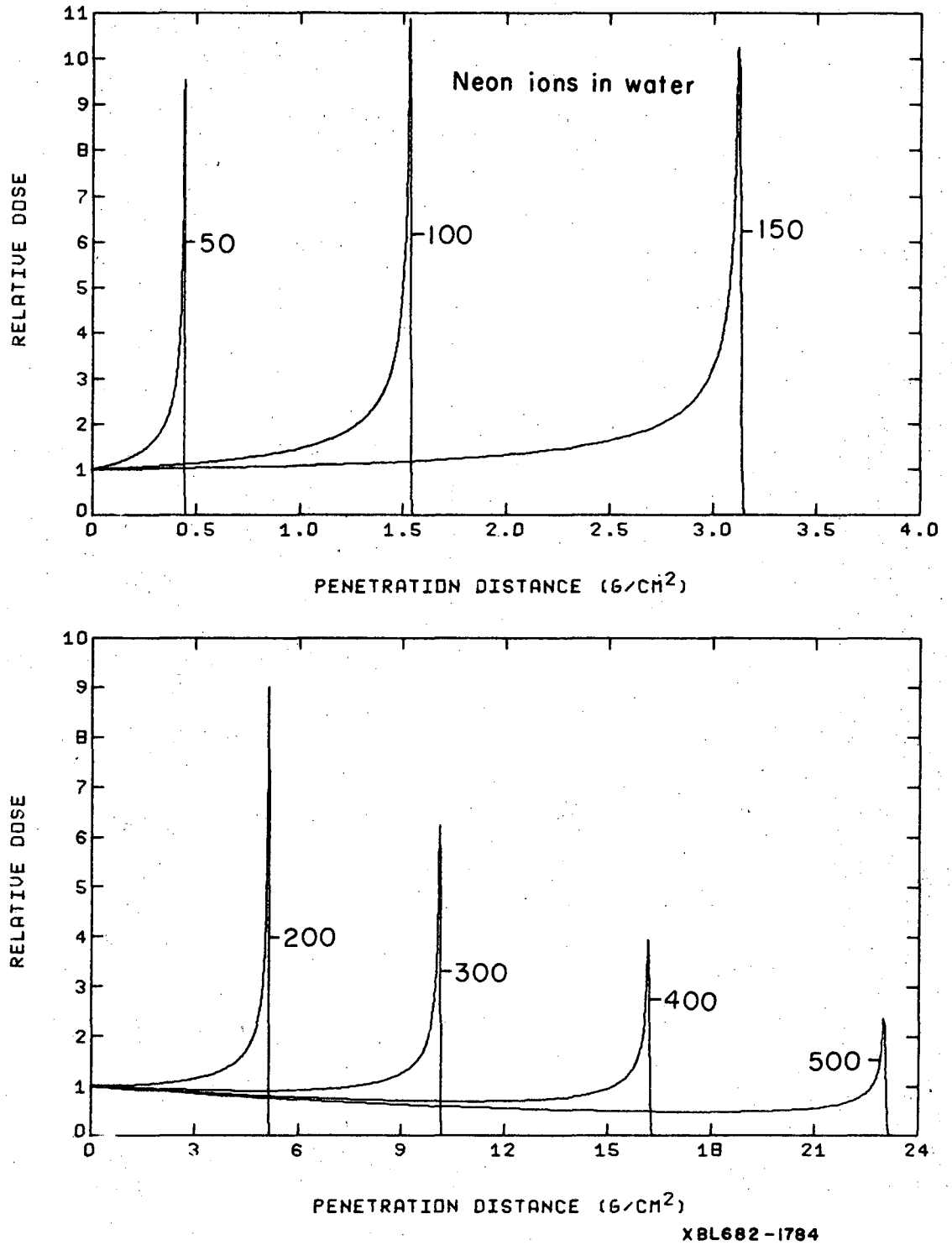

Fig. 17. Bragg curves in water for neon ions with initial energies ranging from 50 to 500 MeV/amu.

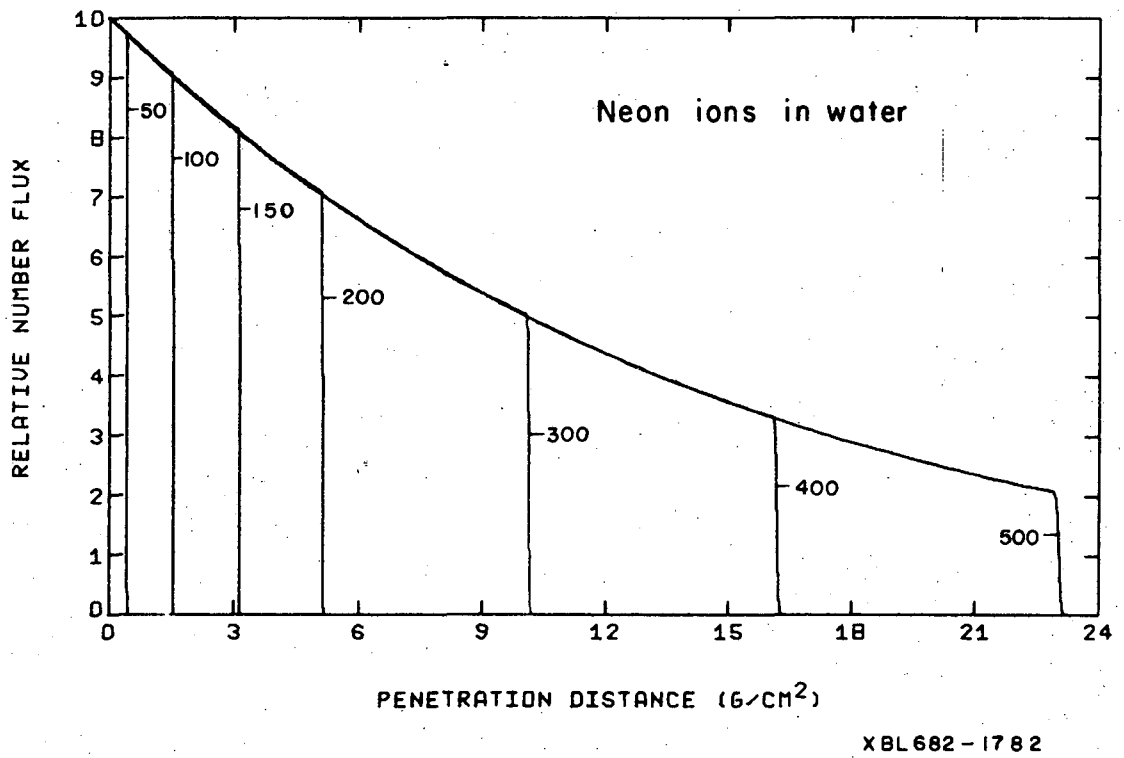

Fig. 18. Flux curves in water for neon ions with initial energies ranging from 50 to 500 MeV/amu.

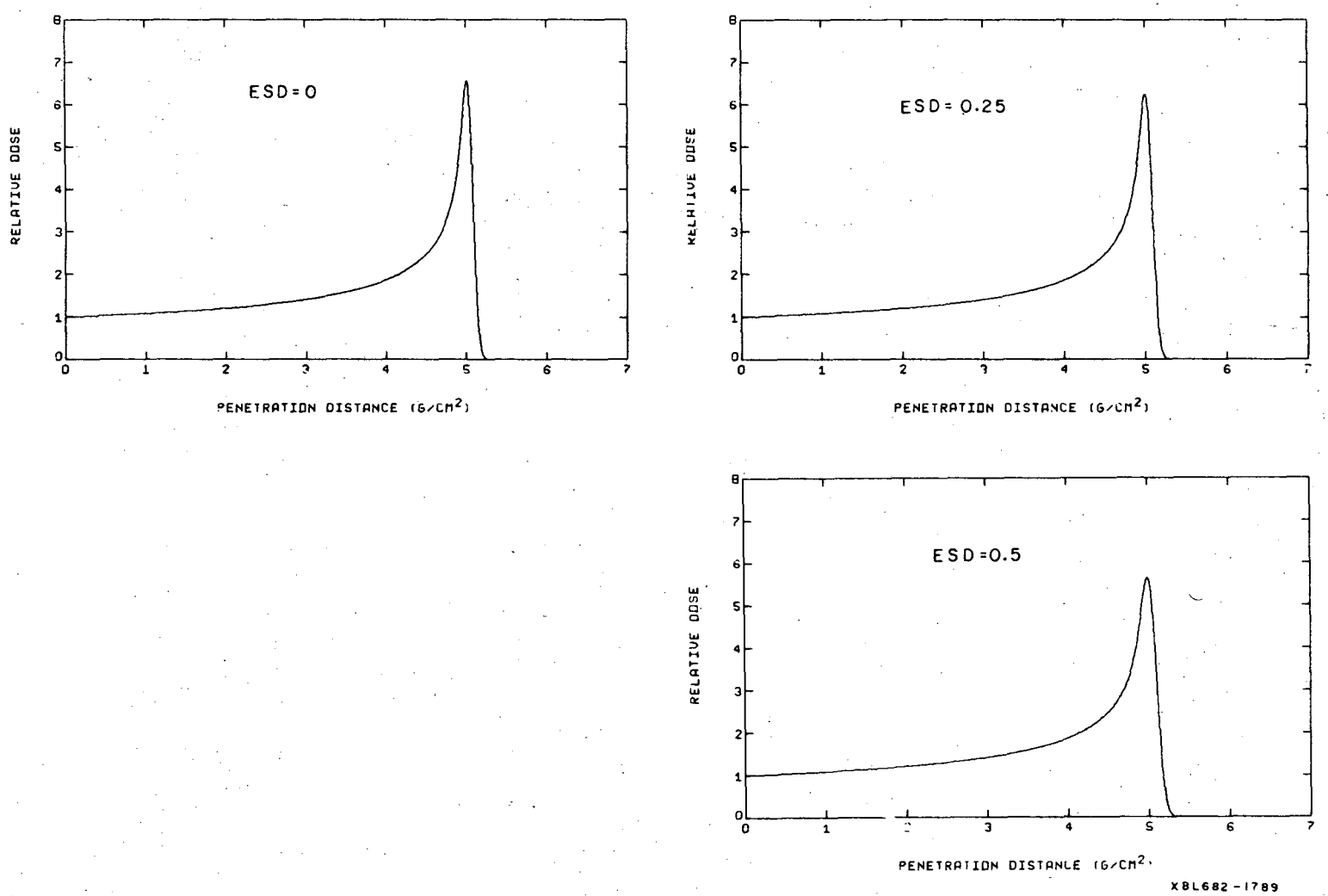

Fig. 19. Bragg curves for protons with a 5 g/cm^2 range in water, for various values of the standard deviation in the initial energy spread.

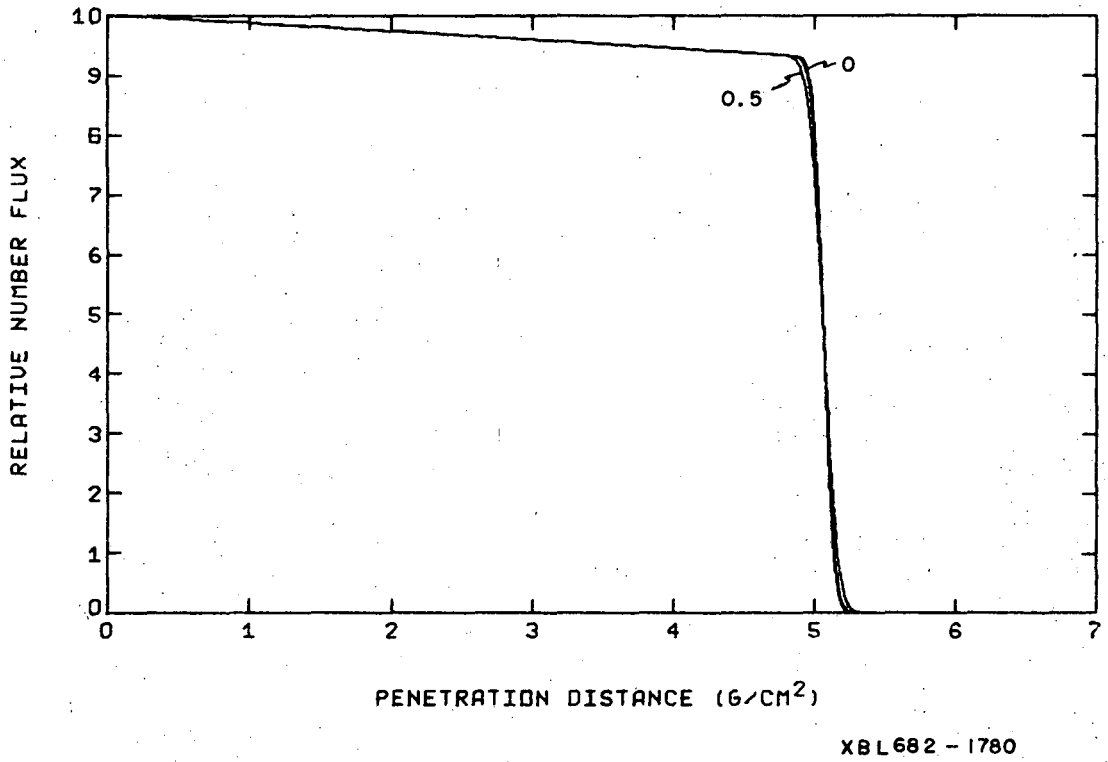

Fig. 20. Flux curves for protons with a 5 g/cm^2 range in water, for various values of the standard deviation in the initial energy spread.

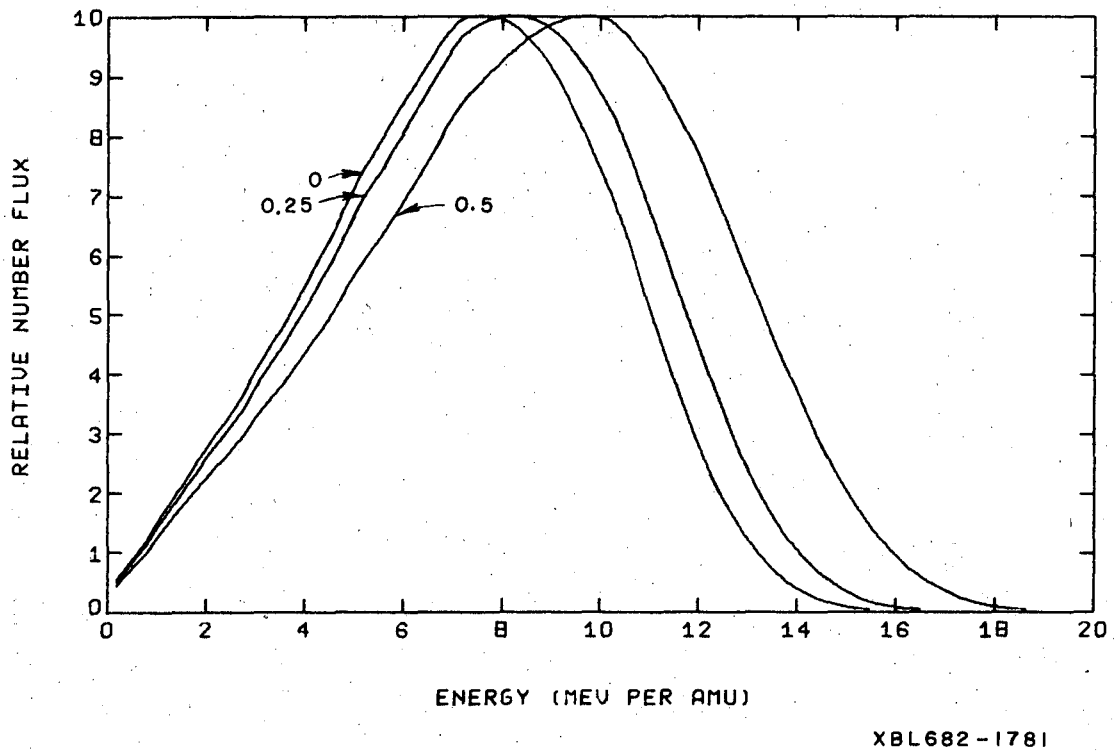

Fig. 21. Spectra at the Bragg peak for protons with a 5 g/cm^2 range in water, for various values of the standard deviation in the initial energy spread.

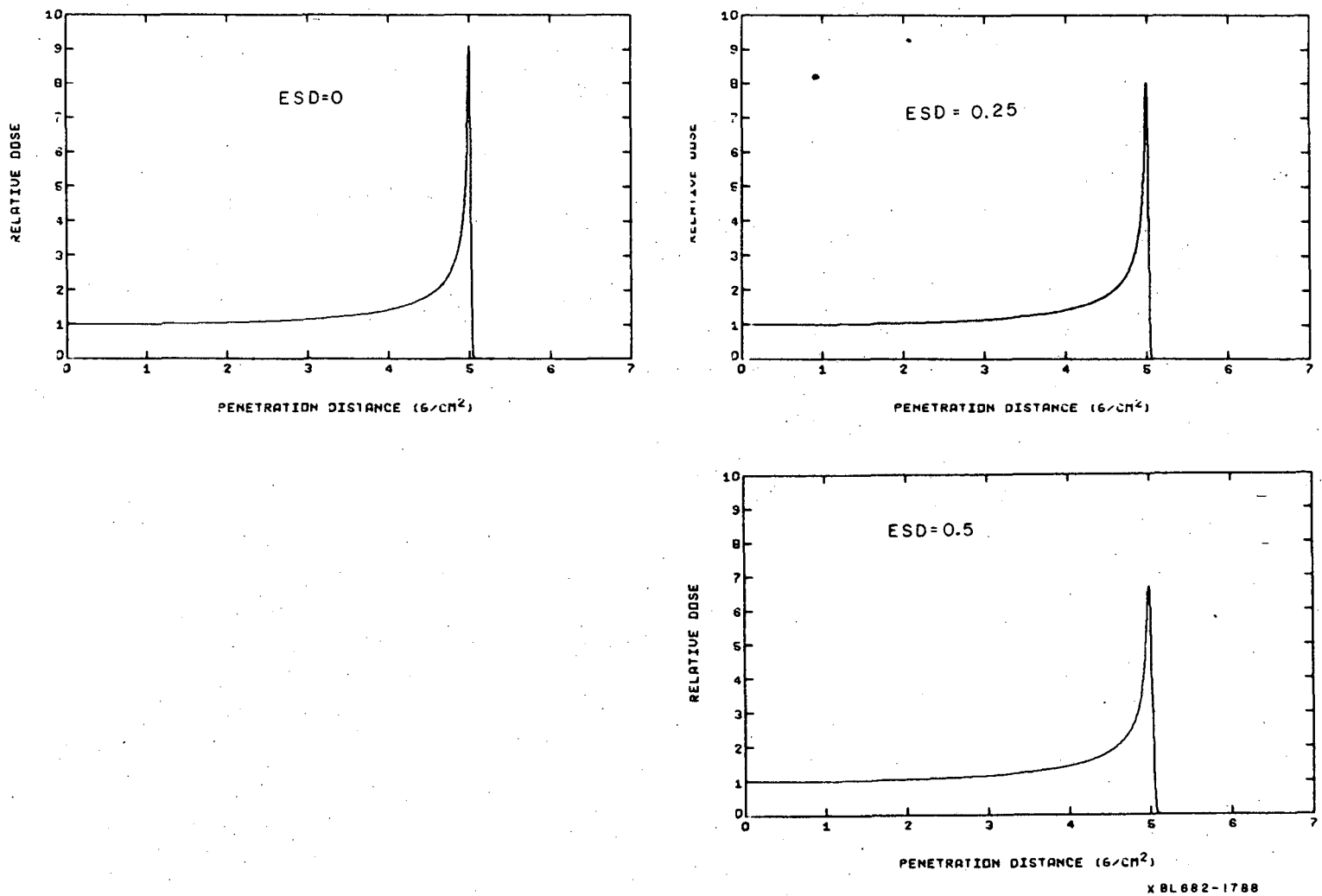

Fig. 22. Bragg curves for neon ions with a 5 g/cm^2 range in water, for various values of the standard deviation in the initial energy spread

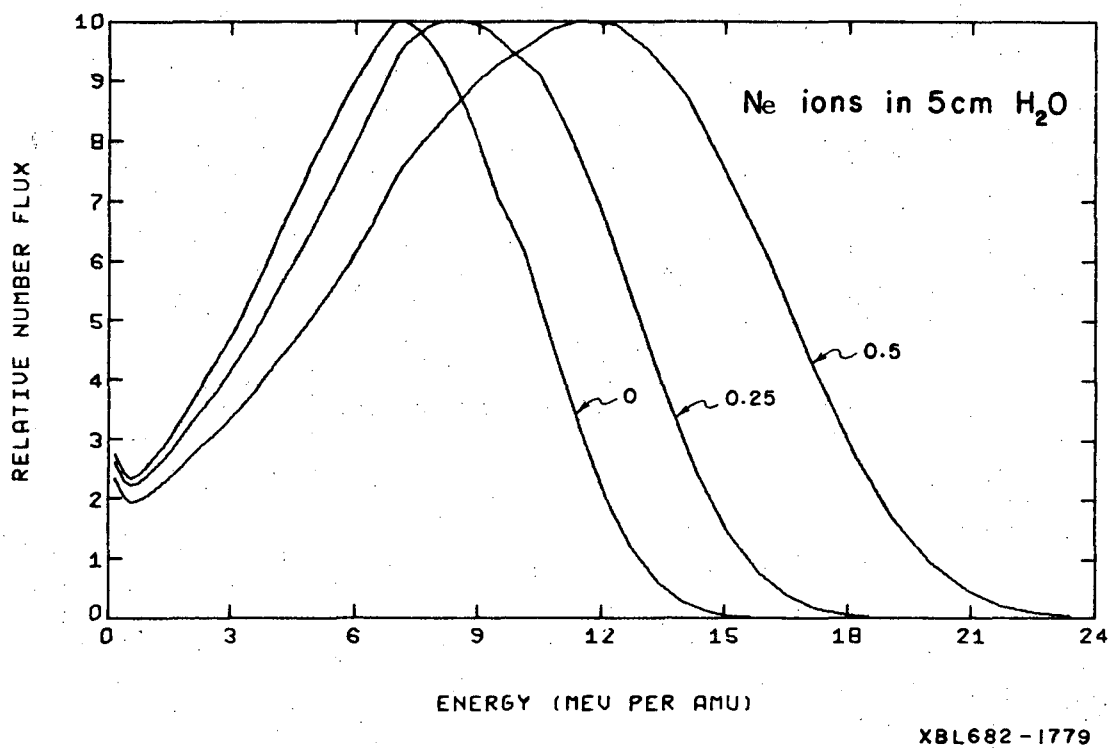

Fig. 23. Spectra at the Bragg peak for neon ions with a 5 g/cm^2 range in water, for various values of the standard deviation in the initial energy spread.

V. CONCLUSIONS AND RECOMMENDATIONS

The methods developed here for computing Bragg, flux, and spectral curves are extremely flexible, in that the calculations are done directly in terms of energy-dependent functions for the ionization energy loss and total nuclear-reaction cross section. Thus, the method is directly applicable to any situation in which the important energy-loss processes are ionization and nuclear interactions.

The methods are also more general than previous ones, in that they are able to make corrections for multiple scattering for systems in which the lab and c.m. coordinate systems are not equivalent. Also, effects due to initial angular and energy spreads of the beam have been included in a natural manner.

Calculations have demonstrated that the nature of the initial beam can strongly influence the shapes of the Bragg and flux curves for a given range in a specified material, but the average energy at the Bragg peak is found to be relatively insensitive to the type of ion used.

Within experimental uncertainties, excellent agreement is obtained between experimental Bragg, flux, and peak spectral curves and the corresponding theoretically calculated curves.

The resolving of the uncertainty in some of the experimental data presented here as to the presence or absence of singificant events due to secondary particles would be an important contribution.

In all calculations in this work, it was assumed that the various processes, such as ionization energy loss and multiple scattering, led to distributions that could be represented by Gaussians. In general, this assumption is well founded. However, in certain limiting cases, deviations from Gaussian distributions are significant. For example, at very low energies, plural scattering could cause skewing of the angular distribution of the beam particles. It would therefore be useful to examine the limits within which the assumptions of Gaussian distributions are valid, although for this work there is little doubt as to the validity of these assumptions.

One limitation of this work is in the assumption of a single, homogeneous target medium. An extremely useful extension would be to multiple-slab geometry, allowing more realistic representations of physical systems.

Another basic limitation of these results is that they do not include effects due to secondary particles. Research is being carried on in this

direction, and results including these effects are expected in the near future.

Part II

NOTATION

Symbol	Description of Symbol
A_i	Atomic weight of the ith species in the target
A_p	Atomic weight of beam particles
A_t	Atomic weight of target
c	Velocity of light
D	Percentage detour factor
$D(s)$	Dose at distance s, in MeV/sec-gm
E	Beam particle energy, in MeV/amu
E_o	Initial energy of beam particles, in MeV/amu
$E_{c.m.}$	Total energy in the coordinate system, in MeV
E_{tot}	Total energy of a particle, in MeV
e	Electron charge
$\langle \Delta E_o^2 \rangle$	Variance of initial beam-energy distribution
f	Attenuation factor due to beam spreading
$f(E)$	Stopping power, in MeV per g/cm^2
K	Binding-effect correction factor
m_e	Electron mass
M_p	Mass of beam particle
$M_o c^2$	Rest energy per amu, $\approx$ 931 MeV
$M(s,\bar{s})$	Path-length distribution function
n_e	Number of electrons per cm^3 in an absorber
N_a	Avogadro's number
N_i	Atomic density of the ith species in the target, in $atoms/cm^3$
$N_e(E)$	Number of particles of energy E
$N_o(E_o)$	Initial particle flux, in $particles/cm^2$-sec
$N(s)$	Total flux at s, in $particles/cm^2$-sec
$N(E,s)$	Energy flux at s, in particles per unit energy at E, per cm^2-sec
p	Beam particle momentum
$P(\theta)$	Scattering probability
r_a	Atomic radius
r_e	Classical electron radius
r_n	Radius of nucleus
r_o	Nuclear unit radius, in fermis
R	Mean range of particles in g/cm^2
$\langle \Delta R^2 \rangle$	Contribution to variance in path-length distribution due to energy-loss fluctuations

SKT	Effective overlap parameter
s	Distance of travel in an absorber, in g/cm^2
$\bar{s}(E)$	Mean distance traveled by particles of energy E, in g/cm^2
$\langle \Delta s_o^2 \rangle$	Contribution to variance in path-length distribution due to initial energy spread
x	Penetration distance into the target, in g/cm^2
y	Mean beam deflection, in g/cm^2
y_o	Initial beam radius
$\langle y^2 \rangle$	Mean square radial spread, in g/cm^2
$\langle \Delta y_o \rangle^2$	Contribution to the variance in the radial-spread distribution due to initial angular spread
Z_i	Atomic number of the ith species in the target
Z_p	Atomic number of beam particles
Z_t	Atomic number of target
β	Velocity ratio
γ	Beam-particle--target-atom mass ratio
θ	Scattering angle in the c.m. system
θ_1	Lower limit on scattering probability
θ_2	Upper limit on scattering probability
$\lambda\!\!\!^{-}$	Wavelength of beam particles, in cm
ρ	Density of target, in g/cm^3
η	Total microscopic nuclear-reaction cross section
$\sigma(E_o)$	Standard deviation in the range distribution for particles of initial energy E_o
$\sigma(E,E_o)$	Standard deviation in the path-length distribution for particles of energy E
$\Sigma(E)$	Total macroscopic reaction cross section, in cm^{-1}
$\bar{\varphi}$	Mean laboratory-system angle of deflection of beam particles
φ_L	Scattering angle in the laboratory system
φ_o	Standard deviation of initial angular spread
φ_s^2	Mean square change in angle of deflection per unit distance
$\langle \varphi^2 \rangle$	Mean square angle of deflection

REFERENCES

1. N. Bohr, On the Theory of the Decrease of Velocity of Moving Electrified Particles on Passing Through Matter, Phil. Mag., 25, 10 (1913).

2. N. Bohr, On the Decrease of Velocity of Swiftly Moving Electrified Particles in Passing Through Matter, Phil. Mag., 30, 581 (1915).

3. H. A. Bethe, Zur Theorie des Durchgangs Schneller Korpuskularstrahlen Durch Materie, Ann. Physik, 5, 325 (1930).

4. H. A. Bethe, Bremsformel fur Elektronen Relativistischer Geschwindigkeit, Z. Physik, 76, 293 (1932).

5. Niels Bohr, The Penetration of Atomic Particles Through Matter, Mat. Fys. Medd. Dan. Vid. Selsk. 18, 8 (1948).

6. F. Bloch, Zur Bremsung Rasch Bewegter Teilchen Beim Durchgang Durch Materie, Ann. Physik, 16, 285 (1933).

7. J. Lindhard and M. Scharff, Energy Dissipation by Ions in the KeV Region, Phys. Rev. 124, 128 (1961).

8. J. Lindhard, M. Scharff, and H. E. Schiott, Range Concepts and Heavy Ion Ranges (Notes on Atomic Collisions, II) Mat. Fys. Medd. Dan. Vid. Selsk., 33, No. 14 (1963).

9. Walter H. Barkas and Martin J. Berger, Tables of Energy Losses and Ranges of Heavy Charged Particles, in Studies in Penetration of Charged Particles in Matter (National Academy of Sciences-National Research Council Publication 1133,

10. Lee C. Northcliffe, Passage of Heavy Ions Through Matter, in Annual Review of Nuclear Science, V. 13, p. 67, 1963; also reprinted as Appendix B in Studies in Penetration of Charged Particles in Matter, (National Academy of Sciences - National Research Council Publication 1133, Washington, D. C., 1964).

11. Earl K. Hyde, The Nuclear Properties of the Heavy Elements, V. III Fission Phenomena, (Prentice-Hall, Inc., Englewood Cliffs, New Jersey, 1964).

12. N. K. Aras, M. P. Menon, and G. E. Gordon, Ranges of Fragments From Fission of U^{235} with Thermal Neutrons and the Kinetic Energy Deficit, Nuclear Physics 69, 337 (1965).

13. Palmer G. Steward, Stopping Power and Range for Any Nucleus in the Specific Energy Interval 0.01- to 500-MeV/amu in Any Nongaseous Material, (Ph.D. Thesis), UCRL-18127, May 1968.

14. R. D. Evans, The Atomic Nucleus (McGraw-Hill Book Co., New York, 1955).

15. Gerald M. Litton, John Lyman, and C. A. Tobias, Penetration of High-Energy Heavy Ions, with the Inclusion of Coulomb, Nuclear, and Other Stochastic Processes, UCRL-17392 Rev., May 1968.

16. H. W. Lewis, Phys. Rev. 85, 599 (1951).

17. F. Bloch, Z. Physik 81, 363 (1938).

18. J. Blatt and V. Weisskopf, Theoretical Nuclear Physics, (John Wiley and Sons, New York, 1952).

19. V. L. Fitch and J. Rainwater, Phys. Rev. 92, 789 (1953).

20. J. A. Wheeler, Phys. Rev. 92, 812 (1953).

21. A. L. Schawlow and C. H. Townes, Science 115, 284, (1952).

22. I. Perlman and T. J. Ypsilantis, Phys. Rev. 79, 30, (1950).

23. E. C. Pollard, Phys. Rev. 47, 611 (1935).

24. M. M. Shapiro, Phys. Rev. 90, 171 (1953).

25. R. Hofstadter, Ann. Rev. Nucl. Sci. 7, 231 (1957).

26. Bruno Rossi, High Energy Particles (Prentice-Hall, Englewood, Cliffs, N.J., 1956).

27. David Halliday, Introductory Nuclear Physics (John Wiley and Sons, New York, 1955).

28. S. A. Goudsmit and J. L. Sanderson, Phys. Rev. 57, 24 (1940).

29. S. A. Goudsmit and J. L. Sanderson, Phys. Rev. 58, 36 (1940).

30. E. J. Williams, Proc. Roy. Soc. (London) A 169, 591 (1939).

31. Martin J. Berger and Stephen M. Seltzer, Multiple-Scattering Corrections for Proton Range Measurements, in Studies in Penetration of Charged Particles in Matter, NAS-NRC-1133, 1964.

32. G. M. Litton, Program BRAGG, a FORTRAN-IV Program for Calculating Bragg Curves and Flux Distributions, UCRL-17391, Feb. 1967.

ACKNOWLEDGMENTS

This research was supported by the Atomic Energy Commission, in part through its Special Fellowship Program in Health Physics, which is administered by the Oak Ridge Associated Universities, and in part through its support of the Biomedical Division of the Lawrence Radiation Laboratory at Berkeley, California.

We wish to express appreciation to Dr. Cornelius Tobias for his invaluable support of this project.

We are indebted to Mr. H. Wade Patterson and the entire Health Physics Department of the Lawrence Radiation Laboratory at Berkeley for their cooperation and support throughout this research. We especially appreciate the patient help of Mrs. Ellen Cimpher who has rendered such valuable assistance by typing the various drafts of this paper.

This work was done under the auspices of the U. S. Atomic Energy Commission.

LEGAL NOTICE

This report was prepared as an account of Government sponsored work. Neither the United States, nor the Commission, nor any person acting on behalf of the Commission:

A. Makes any warranty or representation, expressed or implied, with respect to the accuracy, completeness, or usefulness of the information contained in this report, or that the use of any information, apparatus, method, or process disclosed in this report may not infringe privately owned rights; or

B. Assumes any liabilities with respect to the use of, or for damages resulting from the use of any information, apparatus, method, or process disclosed in this report.

As used in the above, "person acting on behalf of the Commission" includes any employee or contractor of the Commission, or employee of such contractor, to the extent that such employee or contractor of the Commission, or employee of such contractor prepares, disseminates, or provides access to, any information pursuant to his employment or contract with the Commission, or his employment with such contractor.

TECHNICAL INFORMATION DIVISION
LAWRENCE RADIATION LABORATORY
UNIVERSITY OF CALIFORNIA
BERKELEY, CALIFORNIA 94720